MATERIALS SCIENCE

Theory-guided experimental design in battery materials research

Alex Yong Sheng Eng[1]†, Chhail Bihari Soni[2]†, Yanwei Lum[1], Edwin Khoo[3], Zhenpeng Yao[4], S. K. Vineeth[2], Vipin Kumar[2], Jun Lu[5]*, Christopher S. Johnson[5]*, Christopher Wolverton[6]*, Zhi Wei Seh[1]*

A reliable energy storage ecosystem is imperative for a renewable energy future, and continued research is needed to develop promising rechargeable battery chemistries. To this end, better theoretical and experimental understanding of electrochemical mechanisms and structure-property relationships will allow us to accelerate the development of safer batteries with higher energy densities and longer lifetimes. This Review discusses the interplay between theory and experiment in battery materials research, enabling us to not only uncover hitherto unknown mechanisms but also rationally design more promising electrode and electrolyte materials. We examine specific case studies of theory-guided experimental design in lithium-ion, lithium-metal, sodium-metal, and all-solid-state batteries. We also offer insights into how this framework can be extended to multivalent batteries. To close the loop, we outline recent efforts in coupling machine learning with high-throughput computations and experiments. Last, recommendations for effective collaboration between theorists and experimentalists are provided.

INTRODUCTION

Batteries are an integral component of a sustainable energy future, as they can efficiently store and release intermittent renewable energy on demand (*1*–*3*). The Nobel Prize in Chemistry 2019 was awarded for the development of lithium-ion batteries, which has laid the foundation of a wireless, fossil fuel–free society. Lithium-ion batteries today, which are based on the rocking chair concept where lithium ions shuttle between a pair of intercalation anode and cathode (*4*), have a practical specific energy of approximately 170 to 220 Wh kg^{-1} (*5*). To meet the ever-increasing future demands of electrification and grid storage, the U.S. Department of Energy's Battery500 consortium has targeted to build batteries with specific energy of 500 Wh kg^{-1} (*5*). To achieve this target, we will need to constantly innovate and develop superior battery chemistries capable of higher charge capacities and specific energies/energy densities (Fig. 1, A and B), preferably based on sustainable Earth-abundant raw materials (Fig. 1C). Beyond lithium-ion batteries, the promising candidates include lithium-metal batteries, since lithium has extremely high specific capacity (3861 mAh g^{-1}) and negative reduction potential [−3.0 V versus the standard hydrogen electrode (SHE)] (*4*). To circumvent limited reserves of lithium, another attractive alternative is sodium-metal batteries, as sodium has much higher crustal abundance (more than 1000 times that of lithium) (*4*). Despite their immense promise, lithium-metal and sodium-metal batteries still face multiple challenges that need to be overcome before successful commercialization. Nevertheless, a large proportion of contemporary research in these upcoming battery technologies continues to rely on the Edisonian trial-and-error approach. Such studies are typically conducted in chronological order of material synthesis, electrode and electrolyte fabrication, followed by cell assembly and testing. On the basis of a traditional workflow, reports have suggested that there are likely in excess of 10^{100} permutations just for the selection of active materials and electrolytes (*6*). In cases where positive enhancements to cell performance may be observed, further simulation work could be undertaken to derive an understanding of the underlying structure-property relationships within that particular small chemical space. This begs two potential questions: Could theory be better used to design experiments to reduce our time and resource requirements, and if so, how can we envision a workflow that integrates both theoretical modeling and experimentation in tandem?

To this end, the combination of theory and experiment can help to accelerate scientific and technological development in batteries (Fig. 2) (*7*, *8*). In particular, theory calculations can be used to guide the rational design of experiments, obviating the need for an Edisonian approach. For instance, first-principles calculations can be applied in high-throughput screening of large chemical spaces to predict upcoming battery materials, followed by detailed experimental validation of the most promising candidates in a feedback loop. To understand experimentally observed battery phenomena, theory computations can be used to simulate the structures and properties of less understood battery materials, offering deep insight into fundamental processes that are otherwise difficult to access, such as ion diffusion mechanisms and electronic structure effects. Models and simulations can also predict the state of charge, state of health, and cycle life of batteries, coupled with experimental measurements for real-time evaluation of battery performance. This can enable us to make a precise quantitative assessment about absolute limits for performance, such as the remaining useful life, optimal fast charging rate, and risk of short circuits/premature failures, etc. During the research process, scientists can use theoretical models and simulations to

[1]Institute of Materials Research and Engineering, Agency for Science, Technology and Research (A*STAR), 2 Fusionopolis Way, Innovis, Singapore 138634, Singapore. [2]Department of Energy Science and Engineering, Indian Institute of Technology Delhi, Hauz Khas, New Delhi 110 016, India. [3]Institute for Infocomm Research, Agency for Science, Technology and Research (A*STAR), 1 Fusionopolis Way, Connexis, Singapore 138632, Singapore. [4]The State Key Laboratory of Metal Matrix Composites, School of Materials Science and Engineering, and Center of Hydrogen Science, Shanghai Jiao Tong University, Shanghai 200240, P. R. China. [5]Chemical Sciences and Engineering Division, Argonne National Laboratory, Lemont, IL 60439, USA. [6]Department of Materials Science and Engineering, Northwestern University, Evanston, IL 60208, USA.
*Corresponding author. Email: junlu@anl.gov (J.L.); cjohnson@anl.gov (C.S.J.); c-wolverton@northwestern.edu (C.W.); sehzw@imre.a-star.edu.sg (Z.W.S.)
†These authors contributed equally to this work.

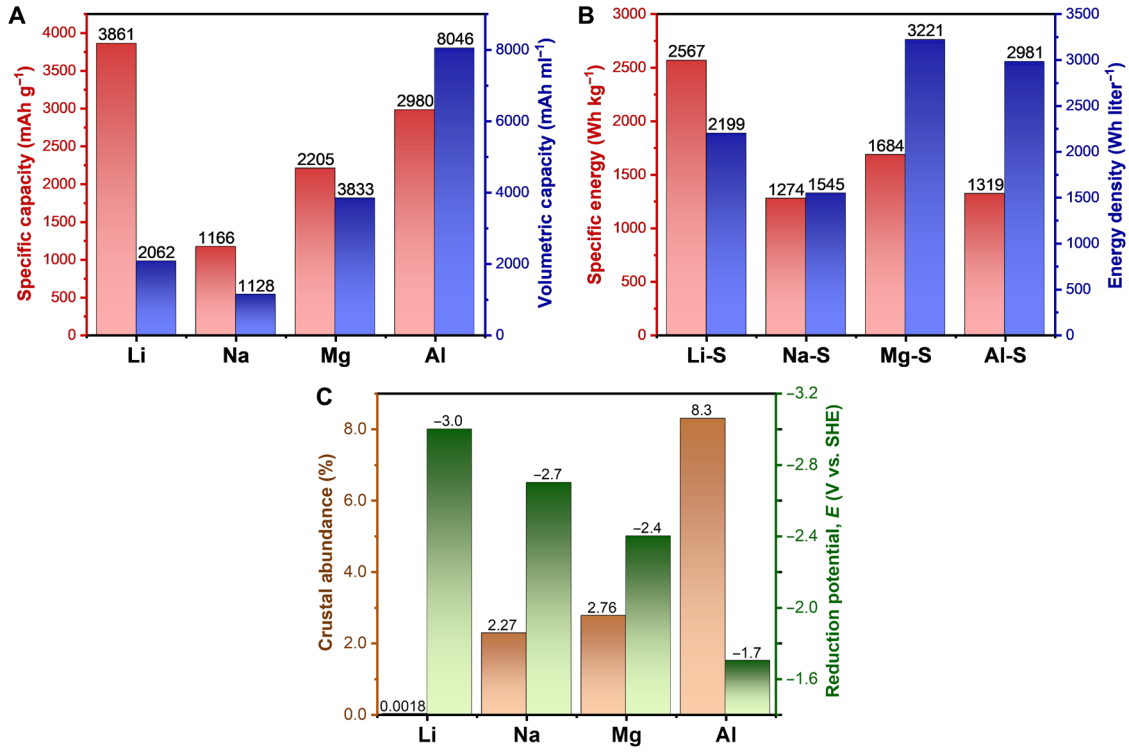

Fig. 1. Summary of the energy storage parameters for various battery chemistries. (**A**) Specific and volumetric capacities of lithium, sodium, magnesium, and aluminum metal anodes. (**B**) Theoretical specific energies and energy densities of metal-sulfur batteries. Tabulated energy values calculated based on the conversion of elemental sulfur, S_8, to the discharged products, i.e., Li_2S, Na_2S, MgS, and Al_2S_3, respectively. (**C**) Elemental abundance in the Earth's crust and reduction potentials of metal anodes versus the standard hydrogen electrode (SHE). Tabulated data for (A) were obtained from (*126*). Data for (B) were obtained from (*19*, *59*, *127*, *128*). Data for (C) were obtained from (*47*, *126*, *129*).

conduct virtual experiments in addition to physical experiments. These "what if" analyses can lend a critical understanding of the battery system in addition to real observed phenomena. Even the most meticulously executed experiments cannot be entirely free from the possibility of human errors in data collection or cognitive bias in data interpretation. In this regard, theory and computational calculations can help with the validation of empirical data, when performed in conjunction with experiments evaluating the real-time electrochemical performance of a cell. Overall, successful integration of computations and experiments can help to establish a predictive framework to understand the complex electrochemical processes occurring in batteries, as well as uncover important underlying trends and common guiding principles in battery materials design. With this deep understanding, we can in turn engineer and control electrochemical reactions to build better batteries.

Theoretical modeling enables us to fundamentally understand the physics and electrochemistry occurring in batteries, especially degradation processes. This includes atomistic models based on density functional theory (DFT) (*9*), molecular dynamics (MD) (*10*), and continuum models such as phase-field models (*11*), single-particle model (*12*), pseudo–two-dimensional (2D) model (*13*), and multiphase porous electrode theory (table S1) (*14*). These models can be used to study a wide variety of battery processes occurring at different length and time scales, including lithium diffusion, dendrite growth, solid electrolyte interphase (SEI) formation/growth, phase separation, and particle cracking. In this review, we focus predominantly on atomistic models using DFT (Fig. 2A) and MD (Fig. 2B) at the materials level. We will also discuss linear stability analysis of continuum models (*15*), which is a mathematical technique that is widely used to study metal plating and dendrite growth (Fig. 2C). In addition, model order reduction is commonly used in reducing the computational complexity of these models to accelerate computation at the expense of some fidelity and accuracy.

Critical to building and validating theoretical models are experimental characterization techniques, preferably in situ and operando (rather than ex situ) to reflect actual operating conditions. Using these techniques, we can quantify key electrochemical, physical, and structural information and connect these parameters to the models. Commonly used experimental techniques can be classified into three main categories, namely, electrochemistry, spectroscopy, and microscopy (table S2). Some typical electrochemical characterization techniques include galvanostatic charge-discharge, electrochemical impedance spectroscopy, galvanostatic/potentiostatic intermittent titration technique, and cyclic/linear sweep voltammetry (Fig. 2E) (*16*). Detailed chemical compositions and environments can be measured using spectroscopic techniques such as Raman, Fourier transform infrared, x-ray absorption/photoelectron, and nuclear magnetic resonance spectroscopy (Fig. 2F) (*17*). To resolve nanoscale and microscale features in battery materials, microscopic techniques such as optical, electron, scanning probe, and x-ray microscopy are used (Fig. 2G) (*18*). Diffraction techniques such as x-ray, electron, and neutron diffraction are also commonly used.

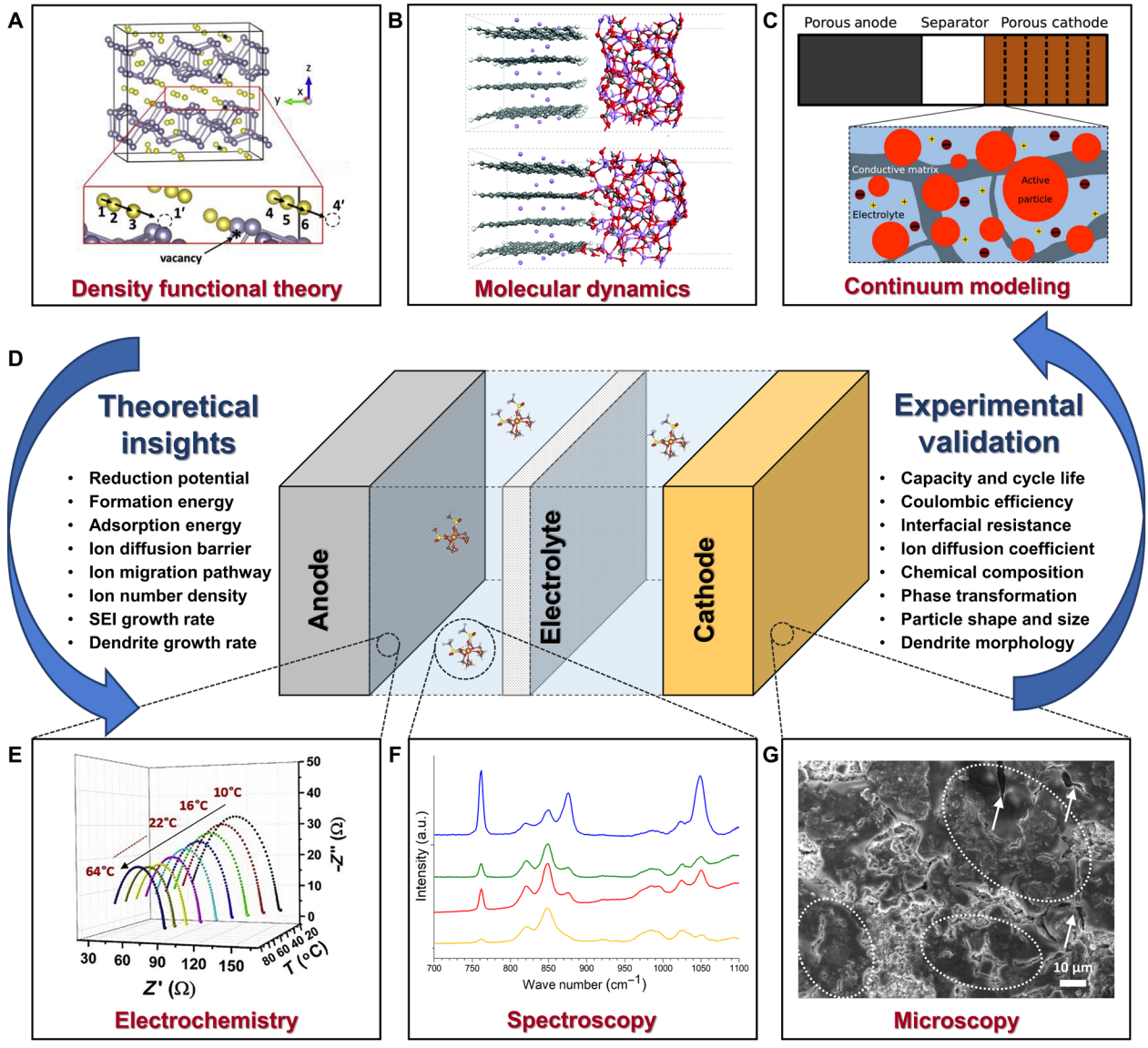

Fig. 2. A framework of theoretical computation and experimentation for building upcoming battery technologies. (**A**) Model structure of a $Na_{1.17}Sn_2$ anode interphase with vacancy defects, as represented by asterisks. Arrows in the magnified view represent possible diffusion paths for Na. (**B**) Calculated MD models of the interface between Li-intercalated graphite (LiC_{24}) anodes and amorphous Li_2CO_3 solid electrolyte interphase (SEI) films for graphite. (**C**) Schematic of a continuum battery model with porous electrodes, based on the multiphase porous electrode theory. (**D**) Schematic representation of standard battery components, and theoretical models on different system length scales, with emphasis on iterations between theoretical insights and experimental validation. (**E**) Electrochemical analysis. Temperature-dependent electrochemical impedance spectra of symmetric sodium cells with a modified biphasic interphase. (**F**) Spectroscopic analysis. Raman spectra of Mg triflate–containing electrolyte solutions. a.u., arbitrary units. (**G**) Microscopic analysis. Scanning electron micrographs of sulfur-composite cathodes in a sodium-sulfur battery, based on a polyvinylidene difluoride binder. Part (A) was adapted with permission from (*51*), Elsevier. Part (B) was reproduced with permission from (*10*), Royal Society of Chemistry. Part (C) was reproduced with permission from (*111*), The Electrochemical Society. Part (E) was adapted with permission from (*50*), Elsevier. Part (F) was reproduced with permission from (*130*), Elsevier. Part (G) was adapted with permission from (*43*), Royal Society of Chemistry.

This review discusses case studies of theory-guided experimental design in battery materials research, where the interplay between theory and experiment led to advanced material predictions and/or improved fundamental understanding. We focus on specific examples in state-of-the-art lithium-ion, lithium-metal, sodium-metal, and all-solid-state batteries. To spur future development, we also offer some perspectives and outlook in the areas of multivalent battery chemistries, understanding battery interfaces, high-throughput computations/experiments, and machine learning. Despite the challenges involved, interdisciplinary collaboration between theorists and experimentalists is expected to yield notable battery advances in the future.

LITHIUM-ION BATTERIES

Traditional lithium-ion batteries operate based on intercalation of lithium ions into layered electrode materials (*3*, *4*). As representative examples, when graphite anode is paired with $LiCoO_2$ and

$LiNi_{1/3}Mn_{1/3}Co_{1/3}O_2$ cathode, these batteries offer theoretical specific energies of 387 and 420 Wh kg^{-1}, respectively (*19*, *20*). Such lithium-ion chemistries have been the mainstream technology for portable electronics and electric vehicles. The combination of theory and experiment over the years has helped us to understand underlying mechanisms and in turn design better lithium-ion batteries.

In 1998, first-principles calculations were used to screen and identify a large class of cathode materials for lithium-ion batteries (*21*). $LiCoO_2$ is a promising cathode material, but the high cost and unethical mining of cobalt have driven the search for alternative elements. In this work, the authors used ab initio calculations to direct the search for alternative cathode materials, where part of the transition metals was replaced with nontransition metals. In particular, it was found that upon replacing cobalt in $LiCoO_2$ with aluminum, the resulting $LiAl_yCo_{1-y}O_2$ material exhibited higher lithium intercalation voltage, with small enough formation enthalpy to form solid solutions. To test the theoretical predictions, $LiAl_yCo_{1-y}O_2$ cathodes were experimentally synthesized and showed higher open circuit and working voltages, while x-ray diffraction and scanning transmission electron microscopy showed that single-phase solid solutions were formed up to $y \approx 0.5$. The cathode material also exhibited reversible charge/discharge behavior for about 10 cycles. Since then, the field of theory-guided experimental design has progressed rapidly with notable advances in computational power and experimental techniques.

Another example where a combination of theory and experiment has led to progress in lithium-ion batteries is the discovery of simultaneous cationic and anionic redox reactions that occur in lithium-excess layered oxide cathode materials. In traditional systems, the transition metal cations in the cathode provide the redox activity required for reversible charging and discharging of the battery. In lithium-excess systems such as $Li_2Ru_{1-y}Sn_yO_3$ and Li_2IrO_3, the oxide anions can also undergo oxidation and subsequent reversible reduction, thereby enabling much higher theoretical capacities (*22*, *23*). To avoid the use of precious metals, other lithium-rich antifluorite compounds, such as Li_5FeO_4, Li_6CoO_4, and Li_6MnO_4, have also been developed (*24*–*26*). As a case in point, Li_5FeO_4 cathodes were studied using both theory and experiment, in which the authors found that reversible cycling relies on both the Fe^{4+}/Fe^{3+} and O^-/O^{2-} redox couples (Fig. 3A) (*27*). In particular, the lithium-excess Li_6-O configuration was identified by DFT calculations to play a key role in enabling the reversible O^-/O^{2-} redox behavior. Density of states calculations led to the finding that O^- in the Li_6-O configuration represents labile oxygen states that can undergo reversible transformation to O^{2-}, which forms the basis of anionic redox in Li_5FeO_4 cathodes (Fig. 3, B to D). Multiple experimental techniques were used for validation, including ex situ Raman spectroscopy (Fig. 3F), x-ray diffraction (Fig. 3G), and x-ray absorption spectroscopy. Simultaneous oxidation of Fe^{3+} to Fe^{4+} and O^{2-} to O^- was experimentally observed at ~3.5 V versus Li/Li^+, upon initial extraction of the first two lithium ions from Li_5FeO_4 (Fig. 3E). Subsequently, the reversible cycling region was identified to be between 1.0 and 3.8 V, which corresponds to the formation of $Li_3FeO_{3.5}$ upon charge and $Li_4FeO_{3.5}$ upon discharge. It was also found that charging beyond 3.8 V led to irreversible formation of Li_2FeO_3, $LiFeO_2$, and O_2 gas due to oxidation of O^- to O^0 and elimination of Li_6-O configurations, hence explaining the drastic capacity decay observed by the authors and in prior literature (*24*, *28*, *29*). This combined theory-experiment work serves as a framework to understand other cation/anion redox materials and provides guiding principles for designing improved lithium-ion battery systems.

LITHIUM-METAL BATTERIES

Lithium-metal batteries can potentially achieve much higher specific energies by the use of a lithium metal anode, with its high specific capacity of 3861 mAh g^{-1} and negative reduction potential of −3.0 V versus SHE (Fig. 1, A and C) (*30*). When lithium anode is paired with a high-capacity cathode material such as sulfur, the resulting lithium-sulfur battery has a theoretical specific energy of 2567 Wh kg^{-1} (Fig. 1B) (*20*). The fundamental difference with intercalation-based lithium-ion batteries is that lithium-sulfur batteries operate based on metal deposition/dissolution at the lithium anode, as well as conversion reaction at the sulfur cathode ($16Li + S_8 \rightleftharpoons 8Li_2S$), hence offering higher specific energy. Besides lithium-sulfur, lithium-oxygen and lithium-air batteries are also emerging technologies because of their high theoretical specific energies. The active material in lithium-air batteries is O_2, with excellent recyclability, less toxicity, and lower associated material costs. Despite these merits, practical application remains elusive because of challenges such as variability in controlling specific discharge products. For instance, discharge products of nonaqueous lithium-air systems include LiOH, Li_2O, and Li_2O_2, which lead to variable theoretical specific capacities of 1117, 1787, and 1165 mAh g^{-1}, corresponding respectively to specific energies of 3350, 5361, and 3495 Wh kg^{-1} based on an average operational potential of 3 V (*31*). Aqueous lithium-air systems in comparison have a much lower specific energy of 2170 Wh kg^{-1} because of the formation of $LiOH{\cdot}H_2O$ as discharge product. In this regard, the air-electrode microstructure is an important determinant of realizable discharge capacities and performance. Hence, despite the promise of these lithium-metal chemistries, challenges must be overcome for their practical adoption to become a reality.

Focusing on the lithium anode, one critical challenge is uncontrolled dendritic growth when lithium is electrodeposited during cycling, thus causing internal short circuits and thermal runaway. Therefore, there has been intensive research on stabilizing the lithium anode via interface and electrolyte engineering, both computationally and experimentally. Within continuum modeling, researchers have performed linear stability analysis of electrodeposition (analysis of how the peaks/troughs of a metal surface grows/shrinks in response to an infinitesimally small surface perturbation). These works mathematically investigate how various transport, electrochemical, and mechanical effects can mitigate or worsen dendritic metal growth in liquid and solid electrolytes, and relate it to experimental techniques that can control such growth (*32*).

As a first example, a combination of theory and experiment was used in the chemomechanical design of lithium-ion conductors coated on polymeric separators to suppress dendrite growth in lithium-metal batteries (*33*). The theoretical foundation that led to this line of work was laid down in studies that used linear stability analysis to analyze the stabilizing and destabilizing effects of surface energy and mechanical factors such as pressure, viscous stress, and deformational stress on electrochemical reaction kinetics (*15*). The main conclusion of this analysis is that solid polymer electrolytes with a sufficiently high shear modulus can block dendritic growth. The analysis was further extended to account for additional density-driven stabilization conferred by the difference in the metal density between the electrode and solid electrolyte (*34*). In this analysis, it

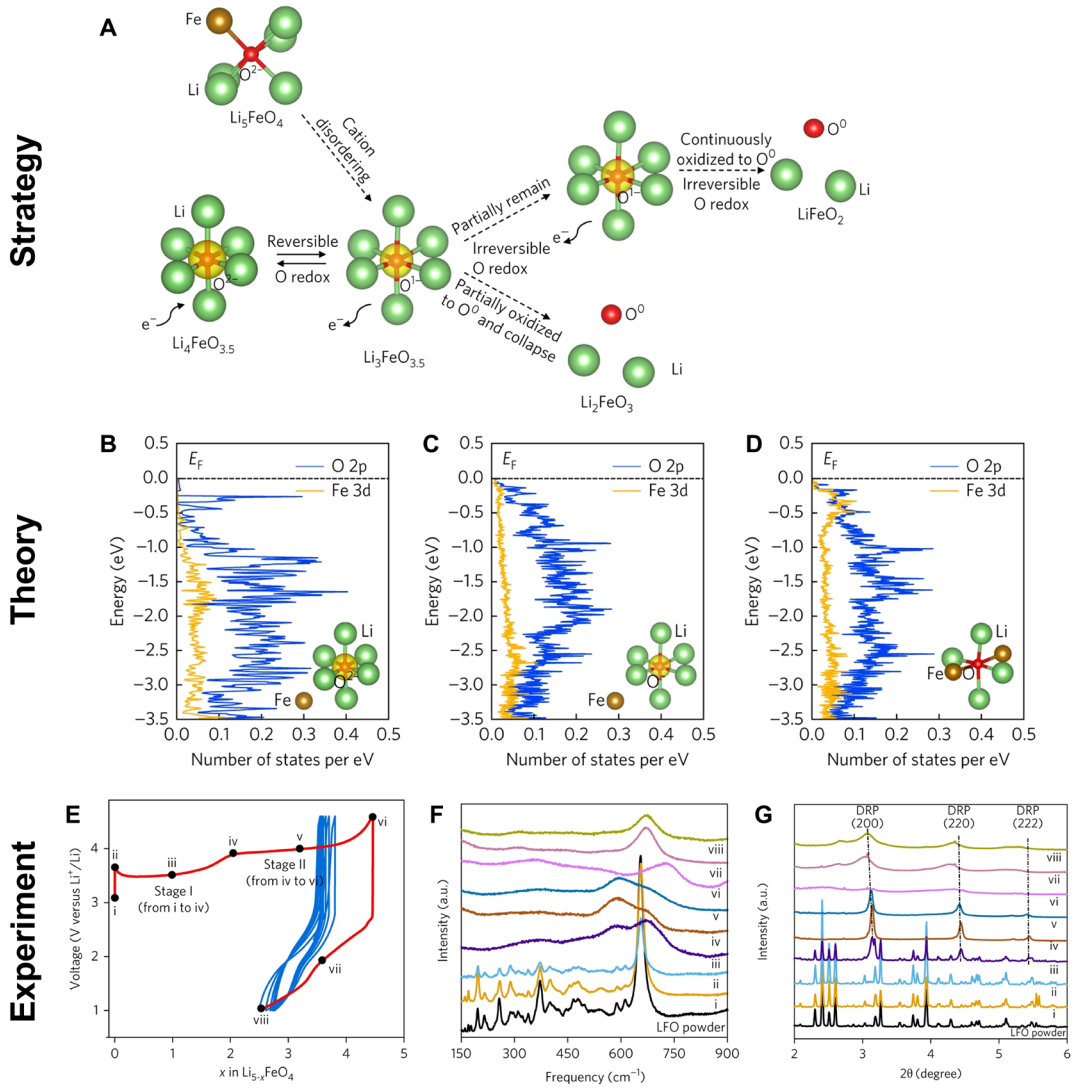

Fig. 3. Phase conversions of Li-rich antifluorite Li_5FeO_4 with simultaneous iron and oxygen redox activity. (**A**) Schematic illustration of the Li_6-O configuration during the delithiation of Li_5FeO_4. Reversible redox reaction of the O^-/O^{2-} couple is maintained when delithiation does not proceed beyond the point where the Li_6-O configuration is destroyed via irreversible oxidation to O^0. (**B** to **D**) Projected density of states from density functional theory simulations of O 2p orbitals and Fe 3d orbitals for O^{2-} ion in the Li_6-O configuration and the nearest Fe ion in cation-disordered $Li_4FeO_{3.5}$ (B), O^{1-} ion in the Li_6-O configuration and the nearest Fe ion in cation-disordered $Li_3FeO_{3.5}$ (C), and O^{2-} ion in the Li/Fe-coordinated O configuration and nearest Fe ions in cation-disordered $Li_3FeO_{3.5}$ (D). (**E**) Charge/discharge behavior of Li_5FeO_4 between 4.7 and 1.0 V. First cycle is shown in red followed by the subsequent five cycles in blue. (**F** and **G**) Ex situ Raman spectra (F) and ex situ high-energy x-ray diffractograms (G) measured at different states of charge/discharge corresponding to the points labeled in (E). The cathode collected at points i and ii shows typical features of the antifluorite Li_5FeO_4, while vertical dashed lines in (G) denote the diffraction peaks corresponding to the (200), (220), and (222) planes of the disordered rock salt phase (DRP). Figure reproduced with permission from (*27*), Springer Nature Limited.

was predicted that such a density-driven stabilization can suppress dendritic growth and be realized by a solid electrolyte that achieves $V_+/V_M < 1$ and $G_s/G_e < 0.7$, where V_+ and V_M are the partial molar volumes of the metal ion in the solid electrolyte and the metal atom in the electrode, respectively, while G_s and G_e are the shear moduli of the solid electrolyte and the electrode, respectively. To access this density-driven stabilization regime, it was suggested that such a solid electrolyte should have ceramic-like ion-conducting domains embedded in a polymer-like matrix with a low shear modulus (*33*). The authors experimentally validated this suggestion by synthesizing LiF on polymer of intrinsic microporosity composites, which were coated onto Celgard separators and used in lithium-metal batteries with liquid electrolyte. These lithium-ion conductors extended the battery cycle lives without short-circuiting, and uniform lithium plating was visually confirmed by synchrotron hard x-ray microtomography.

Another case study of theory-experiment interplay focuses on stabilization of lithium metal anodes in liquid electrolytes via cation regulation (*35*). The lineage of this work can be traced back to an early study that performed a steady-state linear stability analysis of metal electrodeposition/plating in the presence of immobilized anions in a liquid electrolyte (*36*). In this work, the authors concluded that the negative background charge of the tethered anions provides

stabilization to electrodeposition by weakening the electric field at the negative electrode. Generalizing this linear stability analysis, a more recent study (*32*) showed how a negative background charge weakens the electric field at the negative electrode via an ion transport mechanism known as surface conduction (*37*) (current carried by counterions in the electric double layers that is above and beyond the limiting current) and accounted for a transient base state (which enables a detailed examination of the system state around Sand's time) (*38*) and a background charge of any sign. This stability analysis was also validated by experimental results using copper electrodeposition as a model system (*39*). Building on these previous theoretical and experimental results, researchers sandwiched a layer of collagen hydrolysate coated on absorbed glass mat between the metal anode and glass mat separator, achieving uniform lithium electrodeposition/plating in lithium-metal batteries (*35*). This dendrite suppression effect was attributed to a combination of surface conduction stabilization from the negatively charged collagen hydrolysate ions and favorable binding interactions between lithium ions with collagen hydrolysate particles adsorbed on the negative electrode surface (*32*).

Developing 3D current collectors is another method to regulate the electrodeposition of lithium. For example, by integrating theory and experiment, a copper current collector with 3D hollow features that promote the lateral growth of lithium dendrites was designed, reducing dendritic stress and separator damage (Fig. 4, A and B) (*40*). Numerical simulations based on finite element analysis confirm

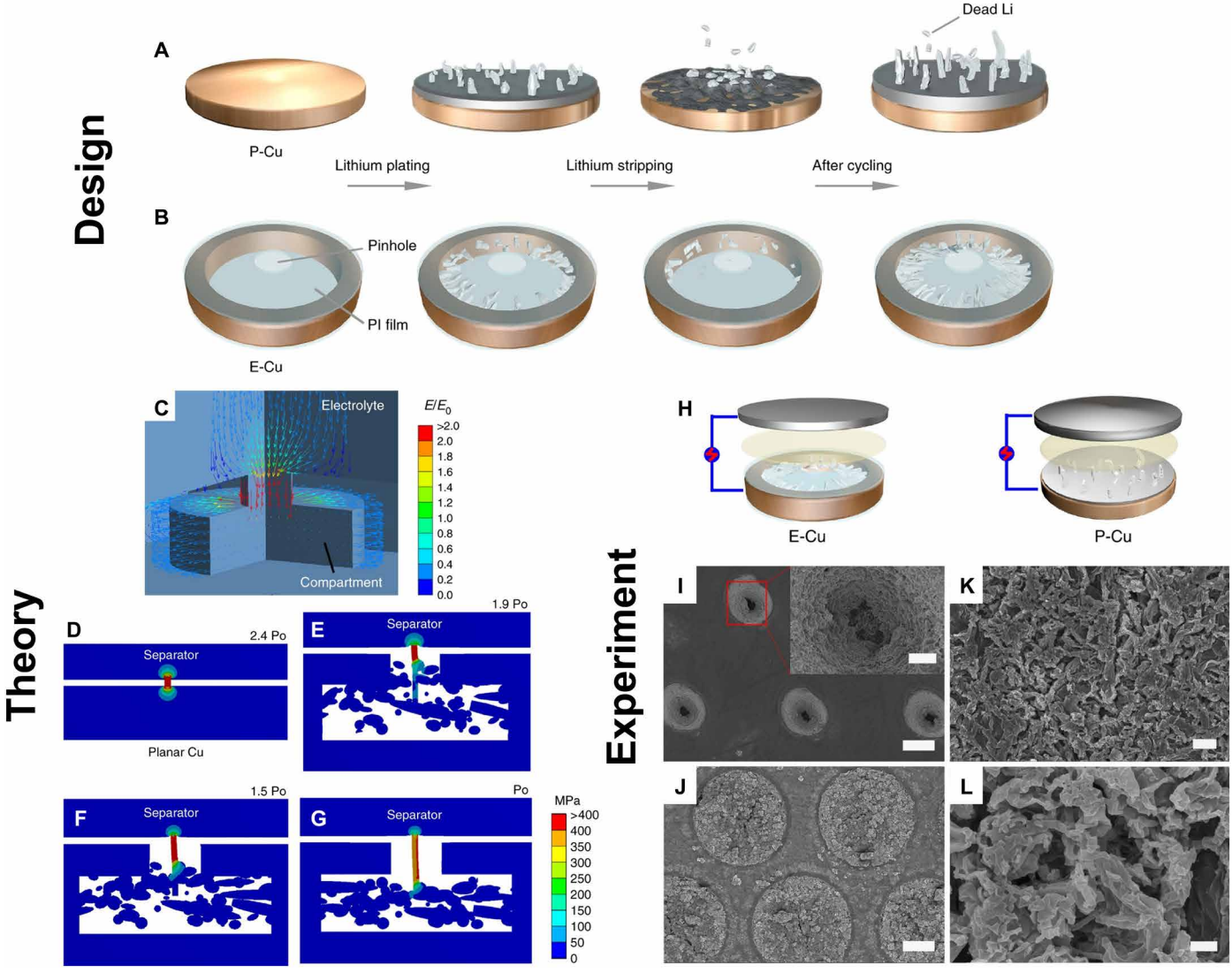

Fig. 4. Numerical simulation–guided design of a 3D current collector for suppressing dendrite growth in Li-metal batteries. (**A** and **B**) Schematic illustration of the formation of different Li anode structures during Li plating/stripping on planar copper [P-Cu, (A)] and a polyimide-clad copper grid current collector [E-Cu, (B)]. (**C**) Numerical simulation of the electric field distribution in E-Cu by an electrical conduction model. (**D** to **G**) Simulations of von Mises stress distributions for dendritic protrusions in a standard case with planar electrode (D), and for E-Cu, where the dendrite layer reaches 95% (E), 75% (F), and 50% (G) of the compartment height. (**H**) Schematic illustrations of Li metal deposition in E-Cu and P-Cu symmetric cell configurations. (**I**) Top view scanning electron micrograph of E-Cu after cycling for 150 cycles at 0.5 mA cm^{-2}. Inset: Magnified image of the pinhole structure defined by the selected area in red. (**J**) Top view of E-Cu after removal of the upper polyimide film. (**K** and **L**) Top-down views of P-Cu after cycling. Scale bars, 50 μm, 50 μm, 2 μm, and 500 nm in (I), (J), (K), and (L). The scale bar in the inset figure of (I) represents 10 μm. Figures adapted with permission from (*40*), Springer Nature Limited.

that this is a result of lateral electric field lines, due to the unique shape of the current collector (Fig. 4C). Moreover, simulations of the von Mises stress distributions of any potential lithium dendrite protrusions show that they generate less stress on the separator compared to the control case when a flat current collector is used (Fig. 4, D to G). On the basis of this theoretical guidance, the authors experimentally tested the 3D current collector to perform lithium plating and stripping in Li//Cu coin cells, observing superior cycling stability with 99% coulombic efficiency (CE) over 150 cycles at 0.5 mA cm^{-2}. The lithium dendrites were found to be accommodated inside the hollow compartments without protruding out (Fig. 4, H to K). This was in contrast to the control case using a planar current collector, which showed uncontrolled dendrite growth and short-circuiting behavior.

Lithium metal anodes are also prone to undesirable side reactions when paired with sulfur cathodes. In lithium-sulfur batteries, soluble lithium polysulfide intermediates (Li_2S_n; $n = 4$ to 8) generated at the sulfur cathode during cycling dissolve into the electrolyte and irreversibly react with the lithium anode, leading to capacity loss and the shuttle effect, with actual specific energies far lower than its theoretical value (*41*). To solve this challenge, suitable binders can be used in sulfur cathodes to bind the lithium polysulfides and reduce their outward diffusion. Starting from DFT calculations, a series of functional groups in polymeric binders were screened for their affinity toward Li-S· species (which represents the relevant end group in Li_2S_n) (*42*). From the screening results, the authors found that the carbonyl functional group has the highest binding energy with lithium polysulfides and, to this end, they predicted poly(vinylpyrrolidone) to be a promising binder material. Experimentally, they tested and verified this binder to exhibit a more stable lithium-sulfur battery cycling performance over prolonged 500 cycles at 0.2 C (Li//S coin cell with initial specific capacity of 760 mAh g^{-1} and 97% CE), compared to the control case with a conventional polyvinylidene fluoride binder. This methodology of theory-guided binder selection has been successfully implemented in sodium-sulfur batteries as well, where the use of a polyacrylic acid binder resulted in long cycle life of 1000 cycles at 0.5 C (Na//S coin cell with initial specific capacity of 1195 mAh g^{-1} and nearly 100% CE) (*43*).

SODIUM-METAL BATTERIES

Sodium-metal batteries are also gaining attention in the community (*44*, *45*). Despite the lower specific capacity (1166 mAh g^{-1}) and less negative reduction potential (−2.7 V versus SHE) of sodium anode compared to lithium, sodium has the advantages of higher natural abundance and lower cost (Fig. 1, A and C) (*46*, *47*). This makes sodium-metal batteries suitable for large-scale and low-cost stationary applications such as grid storage. Room temperature sodium-sulfur batteries, for instance, can offer a specific energy of 1274 Wh kg^{-1} based on the following reaction: $16Na + S_8 \rightleftharpoons 8Na_2S$ (Fig. 1B) (*47*). Sodium-metal batteries are plagued with challenges similar to their lithium analogs, albeit more severe because of fundamental reasons such as the higher chemical reactivity of sodium metal toward the electrolyte (*46*).

In sodium-metal batteries, nonuniform metal deposition and dendrite formation also lead to severe irreversibility and safety issues (*48*). A potential strategy is to use super-concentrated ionic liquid electrolytes with preconditioning, which has been shown to help alleviate these issues. However, the mechanisms of this process are not well understood. In a recent work, a combination of theory and experiment was used to investigate *N*-methyl-*N*-propylpyrrolidinium bis(fluorosulfonyl)imide (C3mpyrFSI) ionic liquid electrolyte with a high concentration (50 mole percent) of sodium bis(fluorosulfonyl)imide (NaFSI) (*49*). In particular, MD simulations were used to examine the effect of different salt concentrations on the interfacial nanostructure (ion number density profiles) of C3mpyrFSI at potential of zero charge. The interfacial nanostructure (force-distance profiles) of C3mpyrFSI at open circuit potential under various salt concentrations was also probed using atomic force microscopy, which agrees well with the MD results. It was found that this super-concentrated electrolyte results in the formation of a highly aggregated $Na_x(FSI)_y$ molten salt–like structure, leading to improved SEI formation and dendrite-free metal deposition. This work sheds light on the mechanisms of improved cycling with super-concentrated ionic liquid electrolytes and provides important guiding principles for the future development of other solvent-in-salt electrolytes for metal anodes.

Another strategy to improve the reversibility of sodium anodes is to develop artificial interphases to stabilize them. An effective artificial interphase should have high Young's modulus and critical strain to suppress dendrite growth, as well as low ionic diffusion barrier to enable high ionic conductivity. To this end, a biphasic interphase consisting of $NaNH_2$ and NaOH was designed on sodium anode using a solid-vapor approach (Fig. 5, A and B) (*50*). DFT was used in the calculation of stress-strain curves to determine the Young's modulus and critical strain (Fig. 5, D and E), followed by calculation of sodium-ion migration pathways to determine the ionic diffusion barrier (Fig. 5C). Motivated by the computational results, the authors experimentally tested and verified that the $NaNH_2$-NaOH artificial interphase was effective in mitigating dendrite growth and promoting high ionic conductivity, using cryo–transmission electron microscopy (Fig. 5, F to I) and electrochemical impedance spectroscopy, respectively. The interphase allowed stable sodium plating and stripping over 500 cycles at current densities ranging from 1 to 50 mA cm^{-2} in symmetric cell configuration. A highly reversible sodium-sulfur battery was also demonstrated over 500 cycles at 0.5 C (Na//S coin cell with initial specific capacity of 1110 mAh g^{-1} and 99.7% CE). It is noteworthy that this concept of integrating theory and experiment was applied in the development of an artificial metal alloy ($Na_{1.17}Sn_2$) interphase on sodium anode as well, enabling stable sodium-sulfur batteries with similar cycling performance (*51*).

ALL-SOLID-STATE BATTERIES

All-solid-state batteries using solid-state electrolytes have attracted burgeoning interest as a safer alternative compared to traditional flammable liquid electrolytes (*7*, *52*). The solid-state electrolyte may also confer additional mechanical stabilization to mitigate dendritic growth in alkali metal anode (*15*). As a result, tremendous efforts have been made in the pursuit of ultrafast solid-state ionic conductors at room temperature to realize all-solid-state batteries. In designing solid-state electrolytes, key desirable properties include high ionic conductivities at room temperature (preferably >0.1 mS cm^{-1}), electrochemical stability for operation at high voltages (>4.0 V), and low charge-transfer resistances at the interface regions with either electrode, all while providing good mechanical strength and flexibility (*52*).

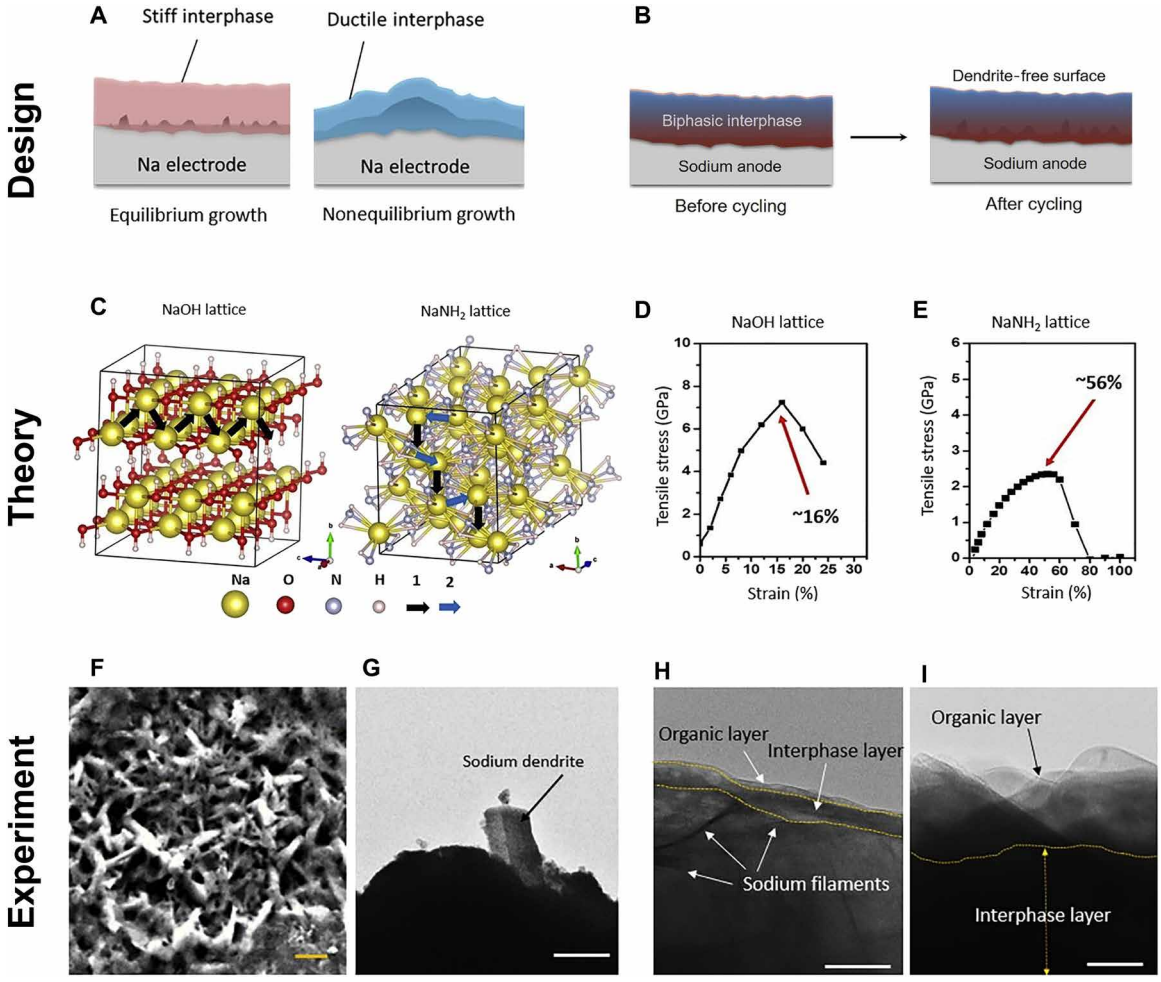

Fig. 5. Theory-guided rational design of a biphasic interphase on sodium-metal anodes with high stiffness and ductility, and a low Na-ion diffusion barrier. (**A**) Illustration of interphase mechanical properties on sodium anodes, specifically a stiff NaOH interphase suppressing large dendrite formation (left), and a ductile $NaNH_2$ interphase accommodating volumetric expansion during sodium growth (right). (**B**) Schematic of a biphasic interphase comprising both stiff and ductile phases maintaining a dendrite-free surface after cycling. (**C**) Models of the NaOH and $NaNH_2$ crystal lattices. Arrows represent thermodynamically favorable ionic diffusion paths predicted by density functional theory calculations. (**D** and **E**) Stress-strain responses of the NaOH (D) and $NaNH_2$ (E) lattices shown in (C). (**F**) Scanning electron micrograph of as-deposited pure sodium (scale bar, 10 μm). (**G**) Cryo–transmission electron micrograph of a sodium dendrite (scale bar, 1 μm). (**H** and **I**) Cross-sectional cryo–transmission electron micrographs of sodium deposition, with biphasic interphase demonstrating both organic and interphase layers. Scale bars, 50 nm (H) and 10 nm (I). Figures adapted with permission from (*50*), Elsevier.

In the field of all-solid-state batteries, various superionic conductors have been reported, which belong to seemingly different structure types, although no universal principle has yet been found. In 2015, a fundamental structural relationship between anion packing and ionic transport in fast lithium-conducting materials was revealed using first-principles–based ion kinetic calculations (*53*). Materials that have underlying body-centered cubic-like anion framework were generally found to be good lithium-ion conductors as they allow direct lithium hops between adjacent tetrahedral sites. These findings provide useful insight and design principles regarding fast ionic transport in lithium-ion conductors. Using this theoretical guidance, researchers were then able to design promising lithium-ion conductors such as $Li_{1+2x}Zn_{1-x}PS_4$ by engineering interstitial defects to further enhance ionic conductivity (*54*).

Having a wide electrochemical stability window is an important design consideration for solid-state electrolytes. Operating outside this window results in decomposition of the solid-state electrolyte, leading to increased cell resistance and lowered performance. However, the mechanisms of this decomposition are not well understood; thus, it has been difficult to predict stability windows. Recently, it was revealed that this stability window is not controlled by the formation energies of the decomposition products (as would be theoretically predicted); instead, it is determined by redox events that occur during (de)lithiation (*55*). Specifically, the authors used a suite of complementary computational and experimental techniques to understand these redox events in argyrodite-type Li_6PS_5Cl solid-state electrolyte. DFT and MD simulations predicted that the kinetically favorable decomposition pathway was indirect instead of direct, via (de) lithiated states of argyrodite, into thermodynamically stable products, hence widening the electrochemical stability window. These theoretical results motivated the use of x-ray diffraction and solid-state nuclear magnetic resonance to observe the (de)lithiated argyrodite

phases, providing clear evidence of the indirect pathway. Notably, the computational and experimental findings were in excellent agreement, lending strong support to the authors' conclusion that the primary mechanism was redox events, which has previously been overlooked. Furthermore, they were able to extend their conclusion to other solid-state electrolytes such as $Li_7La_3Zr_2O_{12}$ garnet-type and $Li_{1.5}Al_{0.5}Ge_{1.5}(PO_4)_3$ NASICON-type, showing the generalizability of their findings.

Another key issue in all-solid-state batteries is the integration between these solid-state electrolytes and the highly reducing alkali metal anodes. Suitable interfaces between the reactive metal anode and solid-state electrolytes need to be developed to prevent the electrolyte material itself from being degraded over time. Recently, a protective passivating hydrate ($Na_3SbS_4{\cdot}8H_2O$) was identified by computation for the solid-state electrolyte Na_3SbS_4 and experimentally verified to serve as a stable electrolyte-anode interface for sodium-metal batteries (Fig. 6, A and B) (*56*). Specifically, first-principles calculations were used to screen possible passivating materials that are stable upon contact with sodium metal, and predicted NaH and Na_2O to be promising candidates. Nudged elastic band calculations were also performed to determine sodium vacancy migration energies of hydrates and identified $Na_3SbS_4{\cdot}8H_2O$ to have good sodium-ion conductivity because of lower migration barriers (Fig. 6, C to E). Experimentally, they synthesized such a layer by exposing Na_3SbS_4 to ambient air, resulting in the formation of a $Na_3SbS_4{\cdot}8H_2O$ hydrate layer. This hydrated phase partially reacts with sodium metal to form NaH and Na_2O as passivating materials, which was confirmed by spatially resolved synchrotron x-ray diffraction (Fig. 6F). They assembled Na//Na_3SbS_4//Na symmetric cells (using in-house–designed pressure cells) and evaluated the sodium plating and stripping performance of the air-exposed case and the pristine case at 0.1 mA cm^{-2}. Consistent with their calculations, they found that the air-treated case resulted in lower and more stable plating and stripping overpotentials (Fig. 6G). On the other hand, the pristine case had continuously increased polarization over a period of 25 hours.

PROSPECTS AND OUTLOOK

In addition to the case studies above, we outline future directions in which similar theory-experiment frameworks can be exploited. These include the development of battery technologies based on multivalent ions, such as magnesium and aluminum ions. In addition, insights

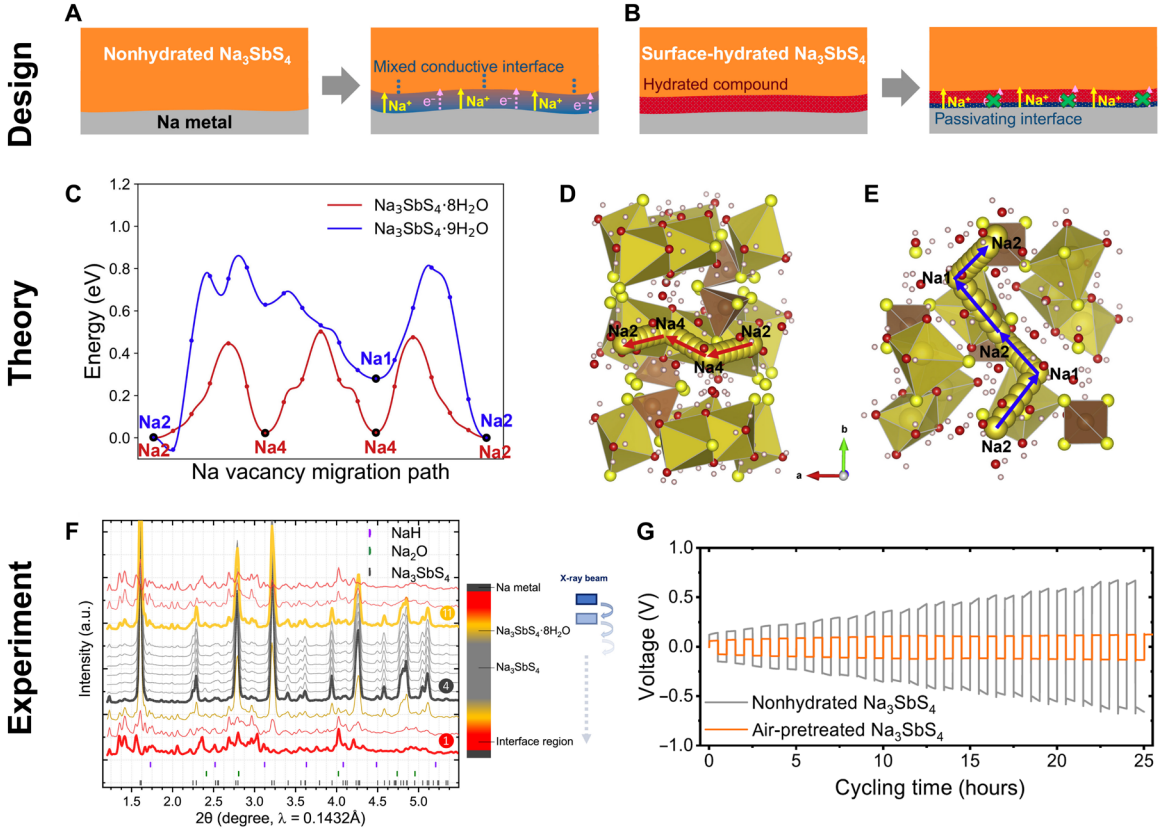

Fig. 6. Enhancement of the interfacial stability between Na anode and the Na_3SbS_4 solid-state electrolyte via surface hydration. (**A** and **B**) Schematic of the electrolyte Na-metal interface for the nonhydrated Na_3SbS_4 solid electrolyte where a mixed conductive layer grew after cycling versus the surface-hydrated Na_3SbS_4 electrolyte where a passivating interface was formed. (**C**) Na vacancy migration energies along the minimum energy paths by nudged elastic band calculations for surface-hydrated Na_3SbS_4 electrolytes: $Na_3SbS_4{\cdot}8H_2O$ and $Na_3SbS_4{\cdot}9H_2O$. (**D** and **E**) Na vacancy migration pathways with minimal percolation barriers in $Na_3SbS_4{\cdot}8H_2O$ along the [100] direction (D) and in $Na_3SbS_4{\cdot}9H_2O$ along the [010] direction (E). $Na(H_2O,S)_6$ octahedra and SbS_4 tetrahedra are respectively colored yellow and brown. (**F**) Experimental validation of the surface-hydrated interface regions in a Na/Na_3SbS_4/Na symmetric cell with spatially resolved post-operando synchrotron x-ray diffractogram. The bolded red, gray, and yellow spectra correspond to the interface region, solid electrolyte, and the hydrated $Na_3SbS_4{\cdot}8H_2O$, respectively. (**G**) Galvanostatic cycling of Na/Na_3SbS_4/Na symmetric cells at a current density of 0.1 mA cm^{-2}, demonstrating increasing potentials for cells without surface hydration pretreatment (gray). Figures adapted with permission from (*56*), Elsevier.

can be gleaned from studying the formation of battery interfaces and their evolution during cycling, where such knowledge may further serve as input for high-throughput computations and machine learning to develop next-generation energy storage systems. Last, we also offer some recommendations for effective and fruitful collaborations between theorists and experimentalists.

Multivalent battery chemistries

Although research has been largely focused on monovalent lithium and sodium batteries, in recent years, there has been emerging interest in developing alternative multivalent chemistries based on magnesium and aluminum (*57*). Compared to lithium, these elements are more earth-abundant; therefore, such batteries are more sustainable and cost-effective in the long term (Fig. 1C). Despite their relatively lower specific capacities, magnesium and aluminum anodes have higher volumetric capacities (3833 and 8046 mAh ml^{-1}, respectively) compared to lithium, due to their capability for multiple electron transfers (Fig. 1A) (*58*). This endows magnesium- and aluminum-sulfur batteries with high energy densities of 3221 and 2981 Wh $liter^{-1}$, respectively (Fig. 1B) (*59*).

Although multivalent battery chemistries come with their own unique mechanisms and challenges, theoretical frameworks and experimental techniques established for studying monovalent batteries can be translated for studying these systems. For example, a cation vacancy-rich anatase TiO_2 was developed that enables reversible magnesium and aluminum ion insertion (*60*). The authors began by performing DFT calculations, which revealed that the intercalation energy of these ions becomes more negative in the presence of single and double titanium vacancies. Motivated by these findings, they intentionally engineered these vacancies into TiO_2 via the introduction of fluoride and hydroxide anions. High-resolution transmission electron microscopy offered atomic resolution of these vacancies in TiO_2. Notably, by using state-of-the-art high-energy x-ray and nuclear magnetic resonance techniques, the authors found that the number of magnesium ions intercalated directly matched the concentration of titanium vacancies, which affirmed their design strategy. Their findings were further validated experimentally by the galvanostatic intermittent titration technique, which confirmed faster Mg^{2+} diffusion in the vacancy-engineered $Ti_{0.78}\square_{0.22}O_{1.12}F_{0.40}(OH)_{0.48}$ as compared to stoichiometric TiO_2. A similar trend was found for aluminum ions, with the presence of titanium vacancies leading to an increase in capacity. These findings motivate the use of theoretical simulations and experimental techniques for defect engineering as a tool to enable reversible multivalent ion intercalation for future studies.

Compared to monovalent batteries, scientific research on multivalent batteries is still in its infancy. The chemistry of magnesium and aluminum electrolytes is considerably more complicated; many promising electrolytes that enable reversible multivalent batteries are chloride-based (*61*, *62*). Hence, the electroactive species are often chloride-containing complex ions in dynamic equilibrium, rather than simply bare metal ions. Examples of such electroactive complexes include $MgCl^+$ and $Mg_2Cl_3^+$ in the case of magnesium aluminum chloride complex electrolyte (*63*, *64*), as well as $AlCl_4^-$ and $Al_2Cl_7^-$ in the case of aluminum chloride in imidazolium chloride–based ionic liquid electrolyte (*65*) (the solvent molecules bonded to these complexes depend on the specific electrolyte solvents used). Experimentally, the identity of these species can be deduced using a variety of techniques including Raman spectroscopy, nuclear magnetic resonance, and single-crystal x-ray diffraction (*66*). For realistic modeling in multivalent batteries, the complex nature of these electroactive species should be taken into account, instead of the simplistic representation of Mg^{2+} and Al^{3+} ions. The combination of theory and experiment will open up opportunities in the discovery of promising multivalent battery materials, including fast charging intercalation/conversion electrodes and high-stability chloride-free electrolytes (*67*).

Understanding battery interfaces

Battery interfaces are arguably the most important yet the least understood component of batteries (*68*). Most of the important reactions occur at the interfaces, for example, the formation and growth of anode-electrolyte interface, cathode-electrolyte interface, and metal dendrites (*69*). These reactions have a profound impact on the degradation and failure of batteries; hence, it is imperative to understand the mechanisms behind interface formation and evolution to engineer more stable interfaces and build safer, long-lasting batteries.

In the scientific literature to date, the majority of battery computations are performed on bulk materials rather than interfaces (*70*). It is well recognized that modeling of battery interfaces is computationally challenging and costly because of the large size and structural complexity of the systems involved (*71*). However, given the importance of interfaces, more efforts should be devoted to such endeavors. For realistic modeling of electrified battery interfaces, we need to take into account both charge and solvent effects (*72*, *73*). Both aspects are often neglected but closely interrelated, for example, the electrolyte needs to be modeled to account for the electrochemical potential. The inclusion of solvation effects is often constrained by computational power: Explicit solvent models are limited by phase-space sampling that is at least 10 times too small to reach convergence, while implicit solvent models do not give a completely realistic picture of the interface (*73*, *74*). As a result, there needs to be a fine balance between the accuracy and cost of the computations involved. To achieve this, efforts should be geared toward the development of methods to reduce computational complexity at the expense of some fidelity (such as model order reduction).

In general, computations on battery interfaces may suffer from lack of validation against experimental data, especially if the results are not directly comparable with one another (*75*). Because of the dynamic nature of battery interfaces, in situ experimental characterization is not trivial as well. Surface-sensitive spectroscopic and microscopic techniques can be used to characterize electrified interfaces; these techniques should preferably be operando and potential dependent as well to give useful information about the surface state under operating conditions (*76*). For example, ambient pressure x-ray photoelectron spectroscopy can be used to characterize the chemical species present at solid-liquid interfaces under more realistic conditions (*77*). Scanning probe microscopy methods such as scanning electrochemical microscopy can also be applied to study the local electrochemical behavior and surface reactivity of battery interfaces with high resolution (*78*). Liquid-phase transmission electron microscopy is emerging as a promising technique to observe SEI formation in sealed liquid electrolyte cells (*79*). In addition, cryo–electron microscopy has recently been used to study lithium and sodium dendrites at interfaces while preserving their original morphology and electrochemical state (*50*, *51*, *80*). However, operando methods to study battery interfaces remain limited, and some of these techniques may not reflect true operating conditions

(such as formation of artificial hot spots in sealed electron microscopy cells). To this end, more can be done to develop operando characterization techniques with improved capabilities and realistic conditions so as to provide directly comparable experimental data to validate the theoretical models.

Despite its challenges, incorporating theoretical computations with experimental data presents tangible benefits toward a better understanding of electrode interfaces. A combined theory-experiment approach can be especially favorable in studying the cathode-electrolyte interface, which is arguably less well understood compared to the anode-electrolyte interface discussed earlier. One such study focused on the interface between high-voltage spinel-type cathodes ($Li_2NiMn_3O_8$, $Li_2FeMn_3O_8$, and $LiCoMnO_4$) and solid-state oxide electrolytes [$Li_{1.5}Al_{0.5}Ti_{1.5}(PO_4)_3$ and $Li_{6.6}La_3Zr_{1.6}Ta_{0.4}O_{12}$], where high-temperature co-sintering typically done to improve the interfacial contact of the two solid components could inadvertently lead to chemical decomposition (*81*). DFT calculations were used together with differential thermoanalysis, thermogravimetry, and x-ray diffraction to predict the decomposition pathways of the various cathode-electrolyte combinations. The authors reported greater compatibility between spinel materials and the $Li_{1.5}Al_{0.5}Ti_{1.5}(PO_4)_3$ solid electrolyte, compared to garnet-type $Li_{6.6}La_3Zr_{1.6}Ta_{0.4}O_{12}$ due to the formation of insulating products that could increase the interfacial resistance. The compatibility data of these material combinations provide important insights toward designing cathode-electrolyte interfaces with enhanced stability and performance.

High-throughput computations/experiments

High-throughput computational materials science uses advanced electronic structure methods and electrochemistry/thermodynamics principles to design promising materials with the help of supercomputers (*69*, *70*). In the area of batteries, high-throughput computations have been used to screen large compositional spaces for yet undiscovered cathode, anode, and electrolyte materials (*71*, *82*). To achieve completely autonomous materials development, high-throughput methods can be combined with autonomous workflows. In essence, autonomous workflows can link different steps of the high-throughput procedure, troubleshoot errors, and make decisions on the next simulation to perform based on the result of the previous step automatically (*83*, *84*). Examples of such workflows are Atomate (*85*), Fireworks (*86*), Aflow (*87*), OQMD (*88*), MyQueue (*89*), and AiiDa (*90*). A recent work has demonstrated a workflow to investigate the thermodynamic and kinetic properties of battery intercalation electrodes based on descriptors like adsorption energies and diffusion barriers, identifying promising cathode materials for magnesium batteries (*91*). Nonetheless, examples of the use of autonomous workflows in battery computations are still relatively limited. More of such works are needed to accelerate battery computations, especially when it comes to modeling of battery interfaces with sheer number of atoms, facets, and terminations.

In an example of interface modeling, researchers examined the electronic, structural, and free energy properties of lithium-ion migration between a Li_2CO_3 SEI film and the graphite anode by using Car-Parrinello–type DFT-based ab initio MD with the Car-Parrinello molecular dynamics (CPMD) code. The calculations were performed across three aspects, starting from the (i) bulk properties of amorphous Li_2CO_3 and Li-intercalated graphite LiC_{24}, examining the (ii) equilibrium properties of anode-SEI interfaces, followed by the (iii) free energy profiles of lithium-ion migration through these interfaces (*10*). Notably, the effect of the termination groups (e.g., mixed COOH, OH, and H) at the graphite edge was investigated. Calculations of these interfacial structures indicated that mixed COOH terminations had a strong binding with the SEI leading to better wettability, while H terminations had poorer wettability. The free energy profile of Li^+ intercalation from the Li_2CO_3-based SEI to LiC_{24} depicted a barrier of at least 1.2 eV. Also, potential energy profiles of Li^+ between the cathode and anode were evaluated under charge and discharge (Fig. 7C). The model demonstrated that approximation of the charging stage is possible with application of an external electric field through the interface. Under the applied field, calculated free energy profiles showed a barrier of about 0.5 eV during charging, which corroborated with experimental data.

Thus, one practical application of theoretical models is their use to predict battery state variables for battery management systems (*92*). Two important degradation mechanisms include (i) loss of lithium inventory because of their consumption by side reactions and (ii) loss of active material leading to a loss of storage capacity. Such model-based approaches rely on physics-based modeling of the degradation behavior (also referred to as the physics-of-failure model) or by building empirical models to describe the decline of a system. They are typically represented by a complex mechanistic model as a set of differential equations, or an empirical regression model, which may then be used to predict future battery performance by extrapolation. Although many mechanistic models use the Butler-Volmer kinetics to calculate the increased film resistance and rate of side reactions, such developed models are typically restricted to cycle life estimation at fairly low current densities (i.e., 1 C) since transport of lithium ions in the electrolyte is usually disregarded. Given that some model characteristics are temperature-dependent, a coupled thermal-electrochemical model (*93*) may better simulate battery performance at lower C rate over a wider range of temperatures (25° to 40°C). The variations in parameters such as the initial electrode stoichiometry and solid-phase diffusion time constants at varying aging cycles can be used as features for prediction of remaining useful life.

In addition, high-throughput experiments are also crucial in complementing and validating the computations described above. Smart automation and robotics can be applied to generate experimental data in a high-throughput manner (*94*). With high-throughput combinatorial methods, battery materials with different chemical compositions, phases, dopants, and defects can be prepared and characterized (*95*, *96*). Advanced techniques such as 3D printing (additive manufacturing), thin-film sputtering, jet dispensing, pulsed laser deposition, and microplate techniques can be used to synthesize and optimize battery materials (*97*, *98*). High-throughput x-ray diffraction and x-ray fluorescence techniques with automated sample changers can be applied to characterize their phase and chemical composition (*99*, *100*). Electrochemical microfluidic cells can also be assembled, with all the components miniaturized and integrated in a flow-based microfluidic chip, for high-throughput screening of promising cathode, anode, and electrolyte materials (*101*). The ultimate goal and challenge is to be able to integrate all these components into a fully automated and continuous process.

Machine learning

To close the loop required for designing next-generation batteries, the high-quality computational and experimental data can be further applied in machine learning. Doing so would enable inverse

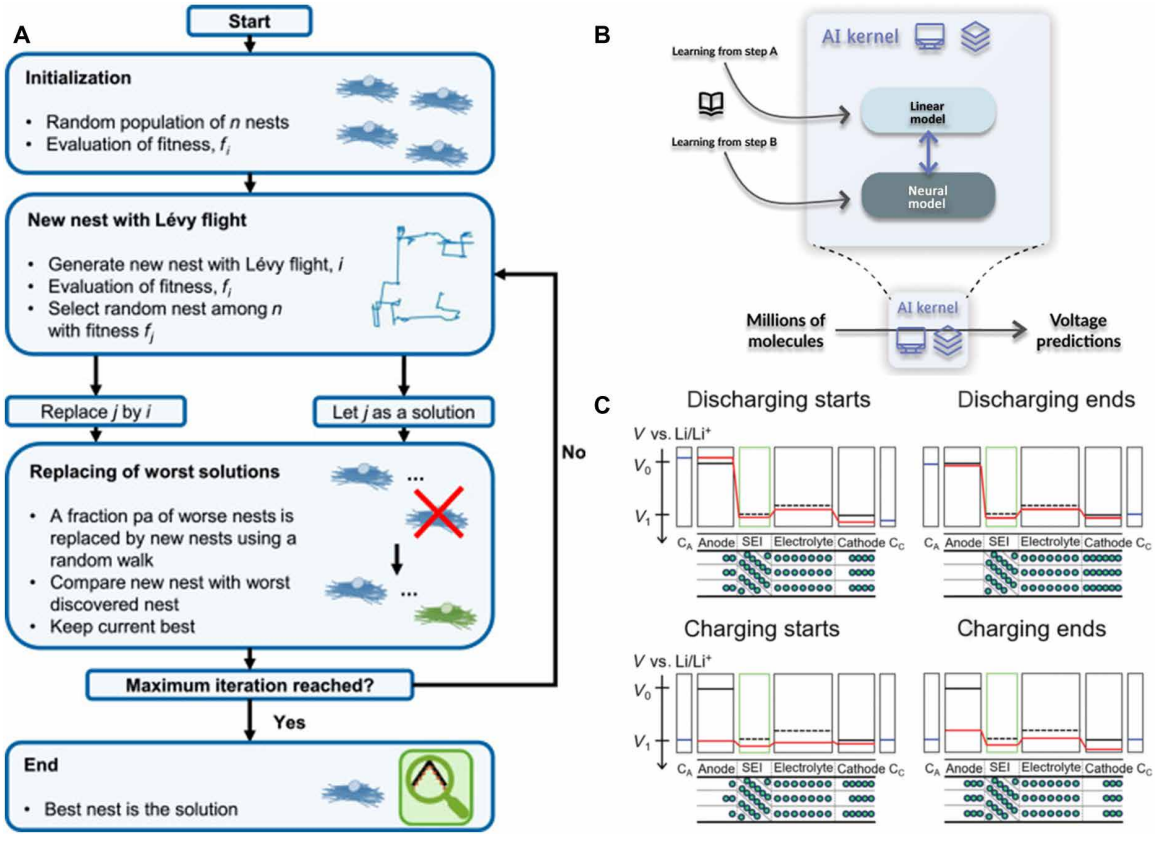

Fig. 7. Recent advances in electrochemical model building and materials discovery. (**A**) Flowchart of the cuckoo search algorithm as a metaheuristic algorithm for parameter identification in electrochemical models, based on the natural brood parasitism of cuckoo birds. Each egg in a nest represents a candidate solution, and the primary task of the algorithm is the production of potentially improved solutions as replacements for the worst solutions of the prior nests. Adapted with permission from (*118*), Elsevier. (**B**) Schematic flow of high-throughput screening and artificial intelligence (AI)–driven prediction of molecules for organic lithium-ion battery cathodes. Adapted with permission from (*119*), Elsevier. (**C**) Schematic representation showing energy profiles of Li^+ during discharging and charging by ab initio MD. Black lines indicate the chemical potential of lithium in the respective materials, while blue lines represent the chemical potential of electrons within the current collector. Red lines indicate the energy profile of Li^+ during the charging or discharging processes. The state of charge within anode and cathode is denoted by the relative amounts of Li^+ (represented by green circles). Adapted with permission from (*10*), Royal Society of Chemistry.

design of batteries (*102*), which allows the battery community to explore the materials space of batteries more efficiently and cheaply. To this end, machine learning algorithms including deep neural networks, support vector machine, and kernel ridge regression (*6*, *103*) have been used to predict the voltage profiles of electrodes, reducing the number of DFT calculations needed to explore the large chemical space (*104*). Another recent report implemented image-based machine learning for microscopic analyses by x-ray computed tomography using deep convolutional generative adversarial networks to produce synthetic 3D images of multiphase microstructures. This method reduced the high computational costs traditionally associated with generating porous 3D structural data, which may in turn be used for predicting performances of large combinations of cathodes based on their actual electrode microstructures (*105*). Furthermore, machine learning has also been applied to screen billions of material candidates and identify promising lithium-ion conductors and solid-state electrolytes (*106*, *107*).

Machine learning has also been used to predict the state of charge, state of health, and cycle life of batteries (*108*), as well as optimize fast charging protocols (*109*). The rise of open-source software in the battery community such as PyBaMM (*110*), MPET (*111*), and phase-field simulation software packages (*112*) will further democratize reproducible research in batteries. However, machine learning models are largely described as "black boxes"; further work is needed to improve the explainability of these models (*113*). This could help to identify underlying latent factors that are chemically meaningful in understanding material properties. Examples of explainable artificial intelligence techniques include layer-wise relevance propagation (*114*), local interpretable model-agnostic explanations (*115*), deep Taylor decomposition (*116*), and Shapley additive explanations (*117*). In the case of deep neural networks, for instance, they are especially suited for machine learning tasks such as image identification (*116*) but suffer from a lack of transparency that restricts the evaluation capability of the solution, therefore limiting the scope of practical applications. In this regard, researchers have introduced a methodology for explaining multilayer neural networks by decomposing the network classification decision into a share of its input elements. This approach can be applied to a comprehensive set of input data, network architecture, and learning tasks, known as deep Taylor decomposition (*116*), which effectively uses the network structure by reversing the data from the output to input layer. Physics and domain knowledge may also be

incorporated into machine learning models to reduce the possibility of overfitting and make the predictions more explainable and interpretable (*108*).

More recently, researchers are also seeking to improve the efficiency of machine learning workflows. One current challenge in the building of electrochemical cell models is parameter identification, due to the typically large number of physical parameters such as diffusion coefficients and reaction rate coefficients, each with varying sensitivity and identifiability. To address this issue, scientists used a data-driven parameter identification technique for an electrochemical model of the lithium-ion battery (*118*), termed as a "cuckoo search algorithm" shown in Fig. 7A. Voltage and current data were used as the sole inputs for multiobjective optimization of parameters. The authors validated the identification framework using commercial lithium nickel manganese cobalt oxide (NMC) cathode pouch cells, reporting that the method increased the identification accuracy of parameters in addition to resolving overfitting issues associated with limited dataset sizes. In another example, a framework was developed by combining artificial intelligence with DFT calculations to accelerate in silico discovery of organic electrode materials (*119*). This framework comprises three steps (Fig. 7B), starting with the resolution of crystal structures of a limited dataset of 28 material candidates (step A) by combining an evolutionary algorithm with DFT calculations, which is then applied to a larger chemical space (step B) of more than 26,000 organic structures from a specific molecular database: Organic Materials for Energy Applications Database (OMEAD). Thus, an efficient artificial intelligence kernel was obtained with good fidelity by combining data from both steps. The kernel allowed high-throughput screening of a large materials library comprising 20 million molecules and identified high-voltage electrode materials containing nitro and nitrile moieties. Moreover, the screening led to the discovery of 459 candidate materials with high theoretical specific energies potentially above 1000 Wh kg^{-1}, thus demonstrating the promise of accelerated discovery using artificial intelligence techniques.

Overall, the combination of high-throughput computations, experiments, and machine learning in a closed loop can open up the prospect of self-driving laboratories for fully autonomous discovery of battery materials (*120*). This paradigm shift will transform and revolutionize the way we carry out battery research in the future.

Recommendations for effective collaboration

Solving complex problems in science often requires interdisciplinary collaboration (*121*). Here, we outline some key lessons that can be learned and discuss best practices for collaboration between theory and experiment in general, which can be applied to other fields beyond batteries as well. The strategies discussed here are by no means exhaustive.

To realize the full potential of theory-guided experimental design, one key lesson is for theorists and experimentalists to collaborate right from the outset (Fig. 8). Often times, theorists and experimentalists engage the help of each other too late into the project, leading to unnecessary delay. In collaborative projects on high-throughput computational screening of battery materials, one common concern is stalled experimental progress at the start since there are no available predictions yet. To maximize efficiency, we recommend experimentalists to begin synthesizing and testing a small subset of these materials while waiting for the calculations to be completed. Regardless of whether these materials exhibit good or poor stability/performance, these experimental results (either positive or negative) are important in validating the initial theoretical models. Subsequently, once a few stable and promising battery materials have been identified theoretically, experimental efforts can be focused on these candidates. This feedback loop between theory and experiment should take place iteratively until the most optimal battery materials have been developed.

On the basis of experience, another key lesson is the importance of generating computational and experimental data that are directly comparable (as far as possible) to facilitate mutual validation. As a

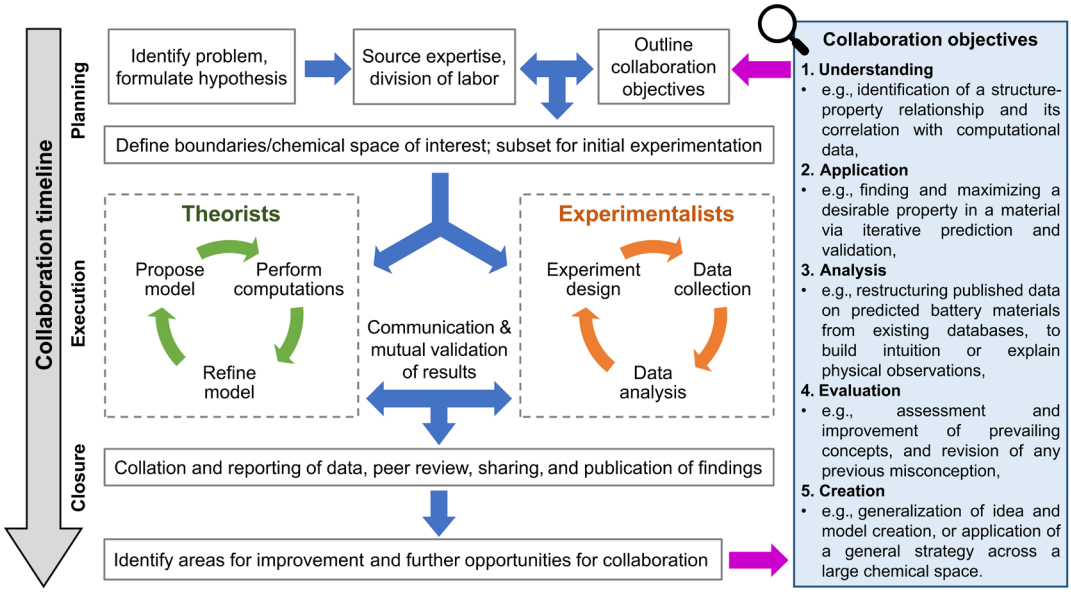

Fig. 8. Workflow for effective collaborations between theorists and experimentalists. Panel on the right describes a proposed classification hierarchy of collaboration objectives, with specific examples, and in order of increasing complexity, labor, or resource requirements and contribution of knowledge to the field of battery development.

simple example, a theory computation performed using a full-cell configuration should not be directly compared to a battery experiment using a half cell configuration, and vice versa. On a similar note, if the theory calculations are performed at 25°C, then the battery cycling experiments should be carried out in a carefully controlled temperature chamber, instead of being left in the laboratory at "room temperature." As another case in point, if the battery experiments involve the presence of a liquid electrolyte, then the theory calculations should ideally incorporate the effects of electrolyte salt and solvent as well. In this respect, theorists and experimentalists should work together to design computations and experiments in tandem. It is therefore crucial to begin a collaboration by first identifying the unique strengths and limitations of each theoretical and experimental technique, recognize specific instances where empirical data generated from a particular technique directly complement the computed results (or vice versa), and then incorporate complementary techniques into the planned workflow from the very start. One example is the use of nudged elastic band computations to calculate ion diffusion barriers within an electrode structure while performing the galvanostatic intermittent titration technique to derive ion diffusion coefficients. Despite the diffusion barrier technically being a different physical parameter from the diffusion coefficient, correlating the observed trends can provide valuable insights to the system. Further nonexhaustive examples of such synergy are summarized in tables S1 and S2. In addition, we outline several works from contemporary literature in table S3, outlining the authors' objectives in performing their theoretical investigations, key experimental findings, and their collective contributions to the field. We hope that these examples may serve to guide upcoming researchers in their experimental design, to better plan and structure theory-guided experimentation efforts.

Effective project management is a critical skill for scientists and is increasingly important in fostering fruitful collaborations as well. From the outset, collaborators should communicate clearly in terms of the project objectives, job scope, milestones, and deliverables. Besides having a well-defined division of labor, unambiguous goals and timelines should also be set. The team should work toward an objective commonly agreed upon, which may range from achieving correlations between observation and prediction, progressively up to generalization and application of a unified idea across different material classes. Borrowing concepts from the taxonomy of learning objectives in education (*122*), we propose a modified classification hierarchy to categorize collaboration objectives in order of increasing complexity, resource requirements, and knowledge contribution to the field (Fig. 8, right) beginning with (i) understanding (e.g., identification of a structure-property relationship and its correlation with computational data), (ii) application (e.g., finding and maximizing a desirable property in a material via iterative prediction and validation), (iii) analysis (e.g., collection and restructuring of published information on predicted battery materials from existing databases such as The Materials Project to build intuition or to explain empirical observations), (iv) evaluation (e.g., assessment and improvement of prevailing concepts with revisions to any previous misconception), and (v) creation (e.g., generalization of idea and creation of a unified model or application of a general strategy across a large chemical space). Such classification levels could potentially aid collaborators and their institutions in resource allocation and project management. In addition to early planning and goal setting, every team member will most likely have different levels of familiarity with one another's expertise at the start. It is important to provide essential background information and explain the computational and experimental methodologies that will be used. At the same time, it is also helpful to be open and frank about the limitations and bottlenecks involved so that everyone is on the same page. For instance, a simple atomistic battery computation may take hours to days to complete on a supercomputer, whereas a long-term battery cycling experiment may take weeks to months. Being cognizant of these differences will help in managing expectations and minimizing conflicts in the future. With rapid developments in battery materials today, research directions or deliverables may change in the course of a project, requiring a consensus on the collaboration objectives (Fig. 8). We believe that when changes and expectations are communicated with timeliness and sensitivity, every collaboration has the chance to span one's entire career.

Last, another key lesson is how to manage huge discrepancies between theoretical and experimental results. In practice, there are inherent limitations in terms of what computations and experiments can do; hence, it is often the case (and perfectly normal) that the theoretical and experimental results do not completely agree with each other. The limitations and challenges of theoretical calculations include errors in commonly used approximations, constraints in length and time scales, and lack of standardized datasets. For instance, DFT calculations suffer from delocalization and static correlation errors due to approximations in the exchange-correlation functional (*123*). Moreover, DFT methods are mainly limited to deal with small atomic systems (few hundreds of atoms) due to the expensive $O(N^3)$ scaling (*124*), while MD methods are also limited to short time scale (picosecond) simulations. Defining a generalized ML descriptor model for designing materials and experimental parameters is also far from reality because the boundary conditions and critical parameters for a system are unique; the lack of standardized datasets in ML further hinders curation and predictability. Similarly, experimental research also suffers from limitations, including the possibility of human error, lack of control over variables, and poor design of experiments. Researchers may misinterpret experimental findings due to a systematic bias toward positive findings. Poor control over extraneous variables may also bias the results and make it difficult for other researchers to reproduce the study. If the theory-experiment discrepancy is too large, it is first important to identify obvious problems that could have arisen, such as errors in mathematical calculations or experimental data analysis, via a systematic process of elimination. This should be followed by an iterative process of refining the theoretical models (such as incorporating electrochemical potential and charge effects in battery calculations) and/or fine-tuning the experimental design (such as eliminating cognitive biases when performing battery experiments). In some cases, the original hypothesis may need to be relooked at and revised. A common pitfall is jumping to conclusions that the theoretical and/or experimental data are outright wrong, which will sour the collaboration. This underscores the importance of having patience in working through the problems together and finding synergy between theory and experiment.

DISCUSSION

Batteries are highly complex and dynamical multicomponent systems, with a multitude of physical phenomena occurring simultaneously during charge and discharge. Here, we have shown specific examples of theory-guided experimental design in battery materials

research, and how this interplay between theory and experiment should take place in a feedback loop until the most promising battery materials have been developed and optimized. Such a theory-experiment framework can also be generalized regardless of the specific type of battery chemistry used, providing universal design principles to develop next-generation monovalent and multivalent batteries. Alongside the increasingly ubiquitous application of artificial intelligence, we envision that data-driven machine learning and high-throughput computations/experiments will be promising for accelerating battery materials design and discovery. To further scientific progress in batteries, it is critical to build offline and online communities to facilitate robust discussions between theorists and experimentalists, especially given the urgent need to pursue a sustainable and green economic recovery in a post–COVID-19 (coronavirus disease 2019) world (*125*). We believe that such concerted theoretical and experimental efforts will bring us closer toward a more secure energy future.

SUPPLEMENTARY MATERIALS

Supplementary material for this article is available at https://science.org/doi/10.1126/sciadv.abm2422

REFERENCES AND NOTES

1. J. M. Tarascon, M. Armand, Issues and challenges facing rechargeable lithium batteries. *Nature* **414**, 359–367 (2001).
2. E. Pomerantseva, F. Bonaccorso, X. Feng, Y. Cui, Y. Gogotsi, Energy storage: The future enabled by nanomaterials. *Science* **366**, eaan8285 (2019).
3. M. S. Whittingham, Ultimate limits to intercalation reactions for lithium batteries. *Chem. Rev.* **114**, 11414–11443 (2014).
4. N. Nitta, F. Wu, J. T. Lee, G. Yushin, Li-ion battery materials: Present and future. *Mater. Today* **18**, 252–264 (2015).
5. Office of Energy Efficiency & Renewable Energy, Battery500: Progress Update (Pacific Northwest National Laboratory, 2020); www.energy.gov/eere/articles/battery500-progress-update.
6. T. Lombardo, M. Duquesnoy, H. el-Bouysidy, F. Årén, A. Gallo-Bueno, P. B. Jørgensen, A. Bhowmik, A. Demortière, E. Ayerbe, F. Alcaide, M. Reynaud, J. Carrasco, A. Grimaud, C. Zhang, T. Vegge, P. Johansson, A. A. Franco, Artificial intelligence applied to battery research: Hype or reality? *Chem. Rev.* (2021).
7. Y. Xiao, Y. Wang, S. H. Bo, J. C. Kim, L. J. Miara, G. Ceder, Understanding interface stability in solid-state batteries. *Nat. Rev. Mater.* **5**, 105–126 (2020).
8. X. Chen, T. Hou, K. A. Persson, Q. Zhang, Combining theory and experiment in lithium–sulfur batteries: Current progress and future perspectives. *Mater. Today* **22**, 142–158 (2019).
9. A. Van der Ven, Z. Deng, S. Banerjee, S. P. Ong, Rechargeable alkali-ion battery materials: Theory and computation. *Chem. Rev.* **120**, 6977–7019 (2020).
10. T. Baba, K. Sodeyama, Y. Kawamura, Y. Tateyama, Li-ion transport at the interface between a graphite anode and Li_2CO_3 solid electrolyte interphase: Ab initio molecular dynamics study. *Phys. Chem. Chem. Phys.* **22**, 10764–10774 (2020).
11. M. Z. Bazant, Thermodynamic stability of driven open systems and control of phase separation by electro-autocatalysis. *Faraday Discuss.* **199**, 423–463 (2017).
12. J. M. Reniers, G. Mulder, D. A. Howey, Review and performance comparison of mechanical-chemical degradation models for lithium-ion batteries. *J. Electrochem. Soc.* **166**, A3189–A3200 (2019).
13. A. Jokar, B. Rajabloo, M. Désilets, M. Lacroix, Review of simplified pseudo-two-dimensional models of lithium-ion batteries. *J. Power Sources* **327**, 44–55 (2016).
14. R. B. Smith, E. Khoo, M. Z. Bazant, Intercalation kinetics in multiphase-layered materials. *J. Phys. Chem. C* **121**, 12505–12523 (2017).
15. C. Monroe, J. Newman, The impact of elastic deformation on deposition kinetics at lithium/polymer interfaces. *J. Electrochem. Soc.* **152**, A396 (2005).
16. Y. Zhu, T. Gao, X. Fan, F. Han, C. Wang, Electrochemical techniques for intercalation electrode materials in rechargeable batteries. *Acc. Chem. Res.* **50**, 1022–1031 (2017).
17. J. Lu, T. Wu, K. Amine, State-of-the-art characterization techniques for advanced lithium-ion batteries. *Nat. Energy* **2**, 17011 (2017).
18. Y. Wu, N. Liu, Visualizing battery reactions and processes by using in situ and in operando microscopies. *Chem* **4**, 438–465 (2018).
19. P. G. Bruce, S. A. Freunberger, L. J. Hardwick, J.-M. Tarascon, Li–O_2 and Li–S batteries with high energy storage. *Nat. Mater.* **11**, 19–29 (2012).
20. Z. W. Seh, Y. Sun, Q. Zhang, Y. Cui, Designing high-energy lithium–sulfur batteries. *Chem. Soc. Rev.* **45**, 5605–5634 (2016).
21. G. Ceder, Y. M. Chiang, D. R. Sadoway, M. K. Aydinol, Y. I. Jang, B. Huang, Identification of cathode materials for lithium batteries guided by first-principles calculations. *Nature* **392**, 694–696 (1998).
22. E. McCalla, M. T. Sougrati, G. Rousse, E. J. Berg, A. Abakumov, N. Recham, K. Ramesha, M. Sathiya, R. Dominko, G. van Tendeloo, P. Novák, J. M. Tarascon, Understanding the roles of anionic redox and oxygen release during electrochemical cycling of lithium-rich layered Li_4FeSbO_6. *J. Am. Chem. Soc.* **137**, 4804–4814 (2015).
23. K. Luo, M. R. Roberts, R. Hao, N. Guerrini, D. M. Pickup, Y. S. Liu, K. Edström, J. Guo, A. V. Chadwick, L. C. Duda, P. G. Bruce, Charge-compensation in 3d-transition-metal-oxide intercalation cathodes through the generation of localized electron holes on oxygen. *Nat. Chem.* **8**, 684–691 (2016).
24. S. Narukawa, Y. Takeda, M. Nishijima, N. Imanishi, O. Yamamoto, M. Tabuchi, Anti-fluorite type Li_6CoO_4, Li_5FeO_4, and Li_6MnO_4 as the cathode for lithium secondary batteries. *Solid State Ion.* **122**, 59–64 (1999).
25. N. Imanishi, Y. Inoue, A. Hirano, M. Ueda, Y. Takeda, H. Sakaebe, M. Tabuchi, Antifluorite compounds, $Li_{5+x}Fe_{1-x}Co_xO_4$, as a lithium intercalation host. *J. Power Sources* **146**, 21–26 (2005).
26. S. Kirklin, M. K. Chan, L. Trahey, M. Thackeray, C. Wolverton, High-throughput screening of high-capacity electrodes for hybrid Li-ion–Li–O_2 cells. *Phys. Chem. Chem. Phys.* **16**, 22073–22082 (2014).
27. C. Zhan, Z. Yao, J. Lu, L. Ma, V. A. Maroni, L. Li, E. Lee, E. E. Alp, T. Wu, J. Wen, Y. Ren, C. Johnson, M. M. Thackeray, M. K. Y. Chan, C. Wolverton, K. Amine, Enabling the high capacity of lithium-rich anti-fluorite lithium iron oxide by simultaneous anionic and cationic redox. *Nat. Energy* **2**, 963–971 (2017).
28. C. S. Johnson, S.-H. Kang, J. T. Vaughey, S. V. Pol, M. Balasubramanian, M. M. Thackeray, Li_2O Removal from Li_5FeO_4: A cathode precursor for lithium-ion batteries. *Chem. Mater.* **22**, 1263–1270 (2010).
29. T. Okumura, M. Shikano, H. Kobayashi, Effect of bulk and surface structural changes in Li5FeO4 positive electrodes during first charging on subsequent lithium-ion battery performance. *J. Mater. Chem. A* **2**, 11847–11856 (2014).
30. D. Lin, Y. Liu, Y. Cui, Reviving the lithium metal anode for high-energy batteries. *Nat. Nanotech.* **12**, 194–206 (2017).
31. T. Liu, J. P. Vivek, E. W. Zhao, J. Lei, N. Garcia-Araez, C. P. Grey, Current challenges and routes forward for nonaqueous lithium–air batteries. *Chem. Rev.* **120**, 6558–6625 (2020).
32. E. Khoo, H. Zhao, M. Z. Bazant, Linear stability analysis of transient electrodeposition in charged porous media: Suppression of dendritic growth by surface conduction. *J. Electrochem. Soc.* **166**, A2280–A2299 (2019).
33. C. Fu, V. Venturi, J. Kim, Z. Ahmad, A. W. Ells, V. Viswanathan, B. A. Helms, Universal chemomechanical design rules for solid-ion conductors to prevent dendrite formation in lithium metal batteries. *Nat. Mater.* **19**, 758–766 (2020).
34. Z. Ahmad, V. Viswanathan, Stability of electrodeposition at solid-solid interfaces and implications for metal anodes. *Phys. Rev. Lett.* **119**, 056003 (2017).
35. J. Zhi, S. Li, M. Han, P. Chen, Biomolecule-guided cation regulation for dendrite-free metal anodes. *Sci. Adv.* **6**, eabb1342 (2020).
36. M. D. Tikekar, L. A. Archer, D. L. Koch, Stability analysis of electrodeposition across a structured electrolyte with immobilized anions. *J. Electrochem. Soc.* **161**, A847–A855 (2014).
37. E. V. Dydek, B. Zaltzman, I. Rubinstein, D. S. Deng, A. Mani, M. Z. Bazant, Overlimiting current in a microchannel. *Phys. Rev. Lett.* **107**, 118301 (2011).
38. P. Bai, J. Li, F. R. Brushett, M. Z. Bazant, Transition of lithium growth mechanisms in liquid electrolytes. *Energy Environ. Sci.* **9**, 3221–3229 (2016).
39. J.-H. Han, M. Wang, P. Bai, F. R. Brushett, M. Z. Bazant, Dendrite suppression by shock electrodeposition in charged porous media. *Sci. Rep.* **6**, 28054 (2016).
40. P. Zou, Y. Wang, S.-W. Chiang, X. Wang, F. Kang, C. Yang, Directing lateral growth of lithium dendrites in micro-compartmented anode arrays for safe lithium metal batteries. *Nat. Commun.* **9**, 464 (2018).
41. Z. W. Seh, W. Li, J. J. Cha, G. Zheng, Y. Yang, M. T. McDowell, P.-C. Hsu, Y. Cui, Sulphur–TiO_2 yolk–shell nanoarchitecture with internal void space for long-cycle lithium–sulphur batteries. *Nat. Commun.* **4**, 1331 (2013).
42. Z. W. Seh, Q. Zhang, W. Li, G. Zheng, H. Yao, Y. Cui, Stable cycling of lithium sulfide cathodes through strong affinity with a bifunctional binder. *Chem. Sci.* **4**, 3673–3677 (2013).
43. A. Y. S. Eng, D. T. Nguyen, V. Kumar, G. S. Subramanian, M. F. Ng, Z. W. Seh, Tailoring binder–cathode interactions for long-life room-temperature sodium–sulfur batteries. *J. Mater. Chem. A* **8**, 22983–22997 (2020).
44. M. D. Slater, D. Kim, E. Lee, C. S. Johnson, Sodium-ion batteries. *Adv. Funct. Mater.* **23**, 947–958 (2013).
45. Y. Zhao, K. R. Adair, X. Sun, Recent developments and insights into the understanding of Na metal anodes for Na-metal batteries. *Energy Environ. Sci.* **11**, 2673–2695 (2018).

46. Z. W. Seh, J. Sun, Y. Sun, Y. Cui, A highly reversible room-temperature sodium metal anode. *ACS Cent. Sci.* **1**, 449–455 (2015).
47. A. Y. S. Eng, V. Kumar, Y. Zhang, J. Luo, W. Wang, Y. Sun, W. Li, Z. W. Seh, Room-temperature sodium–sulfur batteries and beyond: Realizing practical high energy systems through anode, cathode, and electrolyte engineering. *Adv. Energy Mater.* **11**, 2003493 (2021).
48. S. Wei, S. Xu, A. Agrawal, S. Choudhury, Y. Lu, Z. Tu, L. Ma, L. A. Archer, A stable room-temperature sodium–sulfur battery. *Nat. Commun.* **7**, 11722 (2016).
49. D. A. Rakov, F. Chen, S. A. Ferdousi, H. Li, T. Pathirana, A. N. Simonov, P. C. Howlett, R. Atkin, M. Forsyth, Engineering high-energy-density sodium battery anodes for improved cycling with superconcentrated ionic-liquid electrolytes. *Nat. Mater.* **19**, 1096–1101 (2020).
50. V. Kumar, Y. Wang, A. Y. S. Eng, M.-F. Ng, Z. W. Seh, A biphasic interphase design enabling high performance in room temperature sodium-sulfur batteries. *Cell Rep. Phys. Sci.* **1**, 100044 (2020).
51. V. Kumar, A. Y. S. Eng, Y. Wang, D. T. Nguyen, M. F. Ng, Z. W. Seh, An artificial metal-alloy interphase for high-rate and long-life sodium–sulfur batteries. *Energy Storage Mater.* **29**, 1–8 (2020).
52. Q. Zhao, S. Stalin, C.-Z. Zhao, L. A. Archer, Designing solid-state electrolytes for safe, energy-dense batteries. *Nat. Rev. Mater.* **5**, 229–252 (2020).
53. Y. Wang, W. D. Richards, S. P. Ong, L. J. Miara, J. C. Kim, Y. Mo, G. Ceder, Design principles for solid-state lithium superionic conductors. *Nat. Mater.* **14**, 1026–1031 (2015).
54. W. D. Richards, Y. Wang, L. J. Miara, J. C. Kim, G. Ceder, Design of $Li_{1+2x}Zn_{1-x}PS_4$, a new lithium ion conductor. *Energy Environ. Sci.* **9**, 3272–3278 (2016).
55. T. K. Schwietert, V. A. Arszelewska, C. Wang, C. Yu, A. Vasileiadis, N. J. J. de Klerk, J. Hageman, T. Hupfer, I. Kerkamm, Y. Xu, E. van der Maas, E. M. Kelder, S. Ganapathy, M. Wagemaker, Clarifying the relationship between redox activity and electrochemical stability in solid electrolytes. *Nat. Mater.* **19**, 428–435 (2020).
56. Y. Tian, Y. Sun, D. C. Hannah, Y. Xiao, H. Liu, K. W. Chapman, S. H. Bo, G. Ceder, Reactivity-guided interface design in Na metal solid-state batteries. *Joule* **3**, 1037–1050 (2019).
57. M. Li, J. Lu, X. Ji, Y. Li, Y. Shao, Z. Chen, C. Zhong, K. Amine, Design strategies for nonaqueous multivalent-ion and monovalent-ion battery anodes. *Nat. Rev. Mater.* **5**, 276–294 (2020).
58. P. Canepa, G. Sai Gautam, D. C. Hannah, R. Malik, M. Liu, K. G. Gallagher, K. A. Persson, G. Ceder, Odyssey of multivalent cathode materials: Open questions and future challenges. *Chem. Rev.* **117**, 4287–4341 (2017).
59. X. Hong, J. Mei, L. Wen, Y. Tong, A. J. Vasileff, L. Wang, J. Liang, Z. Sun, S. X. Dou, Nonlithium metal–sulfur batteries: Steps toward a leap. *Adv. Mater.* **31**, 1802822 (2019).
60. T. Koketsu, J. Ma, B. J. Morgan, M. Body, C. Legein, W. Dachraoui, M. Giannini, A. Demortière, M. Salanne, F. Dardoize, H. Groult, O. J. Borkiewicz, K. W. Chapman, P. Strasser, D. Dambournet, Reversible magnesium and aluminium ions insertion in cation-deficient anatase TiO_2. *Nat. Mater.* **16**, 1142–1148 (2017).
61. D. Aurbach, Z. Lu, A. Schechter, Y. Gofer, H. Gizbar, R. Turgeman, Y. Cohen, M. Moshkovich, E. Levi, Prototype systems for rechargeable magnesium batteries. *Nature* **407**, 724–727 (2000).
62. M.-C. Lin, M. Gong, B. Lu, Y. Wu, D. Y. Wang, M. Guan, M. Angell, C. Chen, J. Yang, B. J. Hwang, H. Dai, An ultrafast rechargeable aluminium-ion battery. *Nature* **520**, 324–328 (2015).
63. R. E. Doe, R. Han, J. Hwang, A. J. Gmitter, I. Shterenberg, H. D. Yoo, N. Pour, D. Aurbach, Novel, electrolyte solutions comprising fully inorganic salts with high anodic stability for rechargeable magnesium batteries. *Chem. Commun.* **50**, 243–245 (2014).
64. T. Liu, Y. Shao, G. Li, M. Gu, J. Hu, S. Xu, Z. Nie, X. Chen, C. Wang, J. Liu, A facile approach using $MgCl_2$ to formulate high performance Mg^{2+} electrolytes for rechargeable Mg batteries. *J. Mater. Chem. A* **2**, 3430–3438 (2014).
65. T. Jiang, M. C. Brym, G. Dubé, A. Lasia, G. Brisard, Electrodeposition of aluminium from ionic liquids: Part I—Electrodeposition and surface morphology of aluminium from aluminium chloride ($AlCl_3$)–1-ethyl-3-methylimidazolium chloride ([EMIm]Cl) ionic liquids. *Surf. Coat. Tech.* **201**, 1–9 (2006).
66. D.-T. Nguyen, R. Horia, A. Y. S. Eng, S.-W. Song, Z. W. Seh, Material design strategies to improve the performance of rechargeable magnesium–sulfur batteries. *Mater. Horiz.* **8**, 830–853 (2021).
67. M. D. Regulacio, D. T. Nguyen, R. Horia, Z. W. Seh, Designing nanostructured metal chalcogenides as cathode materials for rechargeable magnesium batteries. *Small* **17**, 2007683 (2021).
68. A. Wang, S. Kadam, H. Li, S. Shi, Y. Qi, Review on modeling of the anode solid electrolyte interphase (SEI) for lithium-ion batteries. *npj Comput. Mater.* **4**, 15 (2018).
69. Z. Deng, V. Kumar, F. T. Bölle, F. Caro, A. A. Franco, I. E. Castelli, P. Canepa, Z. W. Seh, Towards autonomous high-throughput multiscale modelling of battery interfaces. *Energy Environ. Sci.* **15**, 579–594 (2022).
70. A. A. Franco, A. Rucci, D. Brandell, C. Frayret, M. Gaberscek, P. Jankowski, P. Johansson, Boosting rechargeable batteries R&D by multiscale modeling: Myth or reality? *Chem. Rev.* **119**, 4569–4627 (2019).
71. W. Fitzhugh, F. Wu, L. Ye, W. Deng, P. Qi, X. Li, A high-throughput search for functionally stable interfaces in sulfide solid-state lithium ion conductors. *Adv. Energy Mater.* **9**, 1900807 (2019).
72. N. N. Rajput, T. J. Seguin, B. M. Wood, X. Qu, K. A. Persson, Elucidating solvation structures for rational design of multivalent electrolytes—A review. *Topics Current Chem.* **376**, 19 (2018).
73. N. Abidi, K. R. G. Lim, Z. W. Seh, S. N. Steinmann, Atomistic modeling of electrocatalysis: Are we there yet? *Wiley Interdiscip. Rev. Comput. Mol. Sci.* **11**, e1499 (2021).
74. S. N. Steinmann, C. Michel, R. Schwiedernoch, P. Sautet, Impacts of electrode potentials and solvents on the electroreduction of CO_2: A comparison of theoretical approaches. *Phys. Chem. Chem. Phys.* **17**, 13949–13963 (2015).
75. S. N. Steinmann, Z. W. Seh, Understanding electrified interfaces. *Nat. Rev. Mater.* **6**, 289–291 (2021).
76. J. Huang, L. Albero Blanquer, J. Bonefacino, E. R. Logan, D. Alves Dalla Corte, C. Delacourt, B. M. Gallant, S. T. Boles, J. R. Dahn, H. Y. Tam, J. M. Tarascon, Operando decoding of chemical and thermal events in commercial Na (Li)-ion cells via optical sensors. *Nat. Energy* **5**, 674–683 (2020).
77. K. Roy, L. Artiglia, J. A. van Bokhoven, Ambient pressure photoelectron spectroscopy: Opportunities in catalysis from solids to liquids and introducing time resolution. *ChemCatChem* **10**, 666–682 (2018).
78. E. Ventosa, W. Schuhmann, Scanning electrochemical microscopy of Li-ion batteries. *Phys. Chem. Chem. Phys.* **17**, 28441–28450 (2015).
79. F. Wu, N. Yao, Advances in sealed liquid cells for in-situ TEM electrochemial investigation of lithium-ion battery. *Nano Energy* **11**, 196–210 (2015).
80. M. J. Zachman, Z. Tu, S. Choudhury, L. A. Archer, L. F. Kourkoutis, Cryo-STEM mapping of solid–liquid interfaces and dendrites in lithium-metal batteries. *Nature* **560**, 345–349 (2018).
81. L. Miara, A. Windmüller, C. L. Tsai, W. D. Richards, Q. Ma, S. Uhlenbruck, O. Guillon, G. Ceder, About the compatibility between high voltage spinel cathode materials and solid oxide electrolytes as a function of temperature. *ACS Appl. Mater. Interfaces* **8**, 26842–26850 (2016).
82. B. Liu, D. Wang, M. Avdeev, S. Shi, J. Yang, W. Zhang, High-throughput computational screening of Li-Containing fluorides for battery cathode coatings. *ACS Sustain. Chem. Eng.* **8**, 948–957 (2019).
83. L. Kahle, A. Marcolongo, N. Marzari, High-throughput computational screening for solid-state Li-ion conductors. *Energy Environ. Sci.* **13**, 928–948 (2020).
84. J. H. Montoya, K. T. Winther, R. A. Flores, T. Bligaard, J. S. Hummelshøj, M. Aykol, Autonomous intelligent agents for accelerated materials discovery. *Chem. Sci.* **11**, 8517–8532 (2020).
85. K. Mathew, J. H. Montoya, A. Faghaninia, S. Dwarakanath, M. Aykol, H. Tang, I. H. Chu, T. Smidt, B. Bocklund, M. Horton, J. Dagdelen, B. Wood, Z. K. Liu, J. Neaton, S. P. Ong, K. Persson, A. Jain, Atomate: A high-level interface to generate, execute, and analyze computational materials science workflows. *Comput. Mater. Sci.* **139**, 140–152 (2017).
86. A. Jain, S. P. Ong, W. Chen, B. Medasani, X. Qu, M. Kocher, M. Brafman, G. Petretto, G. M. Rignanese, G. Hautier, D. Gunter, K. A. Persson, FireWorks: A dynamic workflow system designed for high-throughput applications. *Concurrency Computat. Pract. Exp.* **27**, 5037–5059 (2015).
87. S. Curtarolo, W. Setyawan, G. L. W. Hart, M. Jahnatek, R. V. Chepulskii, R. H. Taylor, S. Wang, J. Xue, K. Yang, O. Levy, M. J. Mehl, H. T. Stokes, D. O. Demchenko, D. Morgan, AFLOW: An automatic framework for high-throughput materials discovery. *Comput. Mater. Sci.* **58**, 218–226 (2012).
88. S. Kirklin, J. E. Saal, B. Meredig, A. Thompson, J. W. Doak, M. Aykol, S. Ruhl, C. Wolverton, The open quantum materials database (OQMD): Assessing the accuracy of DFT formation energies. *npj Comput. Mater.* **1**, 15010 (2015).
89. J. J. Mortensen, M. Gjerding, K. S. Thygesen, MyQueue: Task and workflow scheduling system. *J. Open Source Softw.* **5**, 1844 (2020).
90. S. P. Huber, S. Zoupanos, M. Uhrin, L. Talirz, L. Kahle, R. Häuselmann, D. Gresch, T. Müller, A. V. Yakutovich, C. W. Andersen, F. F. Ramirez, C. S. Adorf, F. Gargiulo, S. Kumbhar, E. Passaro, C. Johnston, A. Merkys, A. Cepellotti, N. Mounet, N. Marzari, B. Kozinsky, G. Pizzi, AiiDA 1.0, a scalable computational infrastructure for automated reproducible workflows and data provenance. *Sci. Data* **7**, 300 (2020).
91. F. T. Bölle, N. R. Mathiesen, A. J. Nielsen, T. Vegge, J. M. Garcia-Lastra, I. E. Castelli, Autonomous discovery of materials for intercalation electrodes. *Batteries Supercaps* **3**, 488–498 (2020).
92. X. Hu, L. Xu, X. Lin, M. Pecht, Battery lifetime prognostics. *Joule* **4**, 310–346 (2020).
93. J. Li, L. Wang, C. Lyu, H. Wang, X. Liu, New method for parameter estimation of an electrochemical-thermal coupling model for $LiCoO_2$ battery. *J. Power Sources* **307**, 220–230 (2016).
94. J.-P. Correa-Baena, K. Hippalgaonkar, J. van Duren, S. Jaffer, V. R. Chandrasekhar, V. Stevanovic, C. Wadia, S. Guha, T. Buonassisi, Accelerating materials development via

automation, machine learning, and high-performance computing. *Joule* **2**, 1410–1420 (2018).
95. P. Liu, B. Guo, T. An, H. Fang, G. Zhu, C. Jiang, X. Jiang, High throughput materials research and development for lithium ion batteries. *J. Materiomics* **3**, 202–208 (2017).
96. Y. Lyu, Y. Liu, T. Cheng, B. Guo, High-throughput characterization methods for lithium batteries. *J. Materiomics* **3**, 221–229 (2017).
97. M. Roberts, J. Owen, High-throughput method to study the effect of precursors and temperature, applied to the synthesis of $LiNi_{1/3}Co_{1/3}Mn_{1/3}O_2$ for lithium batteries. *ACS Comb. Sci.* **13**, 126–134 (2011).
98. S. Maruyama, O. Kubokawa, K. Nanbu, K. Fujimoto, Y. Matsumoto, Combinatorial synthesis of epitaxial $LiCoO_2$ thin films on $SrTiO_3$ (001) via on-substrate sintering of Li_2CO_3 and CoO by pulsed laser deposition. *ACS Comb. Sci.* **18**, 343–348 (2016).
99. S. Vogt, Y. S. Chu, A. Tkachuk, P. Ilinski, D. A. Walko, F. Tsui, Composition characterization of combinatorial materials by scanning X-ray fluorescence microscopy using microfocused synchrotron X-ray beam. *Appl. Surface Sci.* **223**, 214–219 (2004).
100. A. Schiele, T. Hatsukade, B. B. Berkes, P. Hartmann, T. Brezesinski, J. Janek, High-throughput in situ pressure analysis of lithium-ion batteries. *Anal. Chem.* **89**, 8122–8128 (2017).
101. M. A. Modestino, D. F. Rivas, S. M. H. Hashemi, J. G. Gardeniers, D. Psaltis, The potential for microfluidics in electrochemical energy systems. *Energy Environ. Sci.* **9**, 3381–3391 (2016).
102. A. Bhowmik, I. E. Castelli, J. M. Garcia-Lastra, P. B. Jørgensen, O. Winther, T. Vegge, A perspective on inverse design of battery interphases using multi-scale modelling, experiments and generative deep learning. *Energy Storage Mater.* **21**, 446–456 (2019).
103. A. Chen, X. Zhang, Z. Zhou, Machine learning: Accelerating materials development for energy storage and conversion. *InfoMat* **2**, 553–576 (2020).
104. R. P. Joshi, J. Eickholt, L. Li, M. Fornari, V. Barone, J. E. Peralta, Machine learning the voltage of electrode materials in metal-ion batteries. *ACS Appl. Mater. Interfaces* **11**, 18494–18503 (2019).
105. A. Gayon-Lombardo, L. Mosser, N. P. Brandon, S. J. Cooper, Pores for thought: Generative adversarial networks for stochastic reconstruction of 3D multi-phase electrode microstructures with periodic boundaries. *npj Comput. Mater.* **6**, 82 (2020).
106. Y. Zhang, X. He, Z. Chen, Q. Bai, A. M. Nolan, C. A. Roberts, D. Banerjee, T. Matsunaga, Y. Mo, C. Ling, Unsupervised discovery of solid-state lithium ion conductors. *Nat. Commun.* **10**, 5260 (2019).
107. Y. Takagishi, T. Yamanaka, T. Yamaue, Machine learning approaches for designing mesoscale structure of li-ion battery electrodes. *Batteries* **5**, 54 (2019).
108. M.-F. Ng, J. Zhao, Q. Yan, G. J. Conduit, Z. W. Seh, Predicting the state of charge and health of batteries using data-driven machine learning. *Nat. Mach. Intell.* **2**, 161–170 (2020).
109. P. M. Attia, A. Grover, N. Jin, K. A. Severson, T. M. Markov, Y. H. Liao, M. H. Chen, B. Cheong, N. Perkins, Z. Yang, P. K. Herring, M. Aykol, S. J. Harris, R. D. Braatz, S. Ermon, W. C. Chueh, Closed-loop optimization of fast-charging protocols for batteries with machine learning. *Nature* **578**, 397–402 (2020).
110. V. Sulzer, S. G. Marquis, R. Timms, M. Robinson, S. J. Chapman, Python battery mathematical modelling (PyBaMM). *J. Open Res. Softw.* **9**, 14 (2021).
111. R. B. Smith, M. Z. Bazant, Multiphase porous electrode theory. *J. Electrochem. Soc.* **164**, E3291–E3310 (2017).
112. Z. Hong, V. Viswanathan, Open-sourcing phase-field simulations for accelerating energy materials design and optimization. *ACS Energy Lett.* **5**, 3254–3259 (2020).
113. A. B. Arrieta, N. Díaz-Rodríguez, J. Del Ser, A. Bennetot, S. Tabik, A. Barbado, S. Garcia, S. Gil-Lopez, D. Molina, R. Benjamins, R. Chatila, F. Herrera, Explainable artificial intelligence (XAI): Concepts, taxonomies, opportunities and challenges toward responsible AI. *Inf. Fusion* **58**, 82–115 (2020).
114. S. Bach, A. Binder, G. Montavon, F. Klauschen, K. R. Müller, W. Samek, On pixel-wise explanations for non-linear classifier decisions by layer-wise relevance propagation. *PLOS ONE* **10**, e0130140 (2015).
115. M. T. Ribeiro, S. Singh, C. Guestrin, in *Proceedings of the 22nd ACM SIGKDD International Conference on Knowledge Discovery and Data Mining* (Association for Computing Machinery, 2016), pp. 1135–1144.
116. G. Montavon, S. Lapuschkin, A. Binder, W. Samek, K.-R. Müller, Explaining nonlinear classification decisions with deep taylor decomposition. *Pattern Recognit.* **65**, 211–222 (2017).
117. S. Lundberg, S.-I. Lee, An unexpected unity among methods for interpreting model predictions. arXiv:1611.07478 [cs.AI] (22 November 2016).
118. W. Li, I. Demir, D. Cao, D. Jöst, F. Ringbeck, M. Junker, D. U. Sauer, Data-driven systematic parameter identification of an electrochemical model for lithium-ion batteries with artificial intelligence. *Energy Storage Mater.* **44**, 557–570 (2022).
119. R. P. Carvalho, C. F. Marchiori, D. Brandell, C. M. Araujo, Artificial intelligence driven in-silico discovery of novel organic lithium-ion battery cathodes. *Energy Storage Mater.* **44**, 313–325 (2022).
120. F. Häse, L. M. Roch, A. Aspuru-Guzik, Next-generation experimentation with self-driving laboratories. *Trends Chem.* **1**, 282–291 (2019).
121. J. A. Spies, E. A. Perets, K. J. Fisher, B. Rudshteyn, V. S. Batista, G. W. Brudvig, C. A. Schmuttenmaer, Collaboration between experiment and theory in solar fuels research. *Chem. Soc. Rev.* **48**, 1865–1873 (2019).
122. L. W. Anderson, D. R. Krathwohl, B. S. Bloom, P. Airasian, K. Cruikshank, R. Mayer, P. Pintrich, J. Raths, M. Wittrock, *A Taxonomy for Learning, Teaching, and Assessing: A Revision of Bloom's Taxonomy of Educational Objectives, Abridged Edition* (Longman, 2001), vol. 5.
123. A. J. Cohen, P. Mori-Sánchez, W. Yang, Insights into current limitations of density functional theory. *Science* **321**, 792–794 (2008).
124. R. Baer, M. Head-Gordon, Sparsity of the density matrix in Kohn-Sham density functional theory and an assessment of linear system-size scaling methods. *Phys. Rev. Lett.* **79**, 3962–3965 (1997).
125. P. M. Forster, H. I. Forster, M. J. Evans, M. J. Gidden, C. D. Jones, C. A. Keller, R. D. Lamboll, C. L. Quéré, J. Rogelj, D. Rosen, C. F. Schleussner, T. B. Richardson, C. J. Smith, S. T. Turnock, Current and future global climate impacts resulting from COVID-19. *Nat. Clim. Change* **10**, 913–919 (2020).
126. J. Muldoon, C. B. Bucur, T. Gregory, Quest for nonaqueous multivalent secondary batteries: Magnesium and beyond. *Chem. Rev.* **114**, 11683–11720 (2014).
127. X. Xu, D. Zhou, X. Qin, K. Lin, F. Kang, B. Li, D. Shanmukaraj, T. Rojo, M. Armand, G. Wang, A room-temperature sodium–sulfur battery with high capacity and stable cycling performance. *Nat. Commun.* **9**, 3870 (2018).
128. C.-X. Zu, H. Li, Thermodynamic analysis on energy densities of batteries. *Energy Environ. Sci.* **4**, 2614–2624 (2011).
129. A. Russell, K. L. Lee, *Structure-Property Relations in Nonferrous Metals* (John Wiley & Sons, 2005).
130. D.-T. Nguyen, A. Y. S. Eng, M. F. Ng, V. Kumar, Z. Sofer, A. D. Handoko, G. S. Subramanian, Z. W. Seh, A high-performance magnesium triflate-based electrolyte for rechargeable magnesium batteries. *Cell Rep. Phys. Sci.* **1**, 100265 (2020).

Acknowledgments: We thank E. Lee and M. F. Ng for helpful discussions. **Funding:** This work was supported by the Singapore National Research Foundation (NRF-NRFF2017-04) and the U.S. Department of Energy (DOE), Office of Energy Efficiency and Renewable Energy, Vehicle Technologies Office. Argonne National Laboratory is operated for DOE Office of Science by UChicago Argonne, LLC, under contract number DE-AC02-06CH11357. **Author contributions:** All authors contributed to researching data for article, substantial contribution to discussion of content, writing, and review/editing of manuscript before submission. **Competing interests:** The authors declare that they have no competing interests. **Data and materials availability:** All data needed to evaluate the conclusions in the paper are present in the paper and/or the Supplementary Materials.

Submitted 3 September 2021
Accepted 25 March 2022
Published 11 May 2022
10.1126/sciadv.abm2422